IEEE Access
Multidisciplinary | Rapid Review | Open Access Journal

Received July 4, 2016, accepted August 3, 2016, date of publication August 10, 2016, date of current version September 28, 2016.

Digital Object Identifier 10.1109/ACCESS.2016.2599026

Analysis and Optimization of FFR-Aided OFDMA-Based Heterogeneous Cellular Networks

JAN GARCÍA-MORALES, (Student Member, IEEE), GUILLEM FEMENIAS, (Senior Member, IEEE), AND FELIP RIERA-PALOU, (Senior Member, IEEE)

Mobile Communications Group, University of the Balearic Islands, 07122 Palma, Spain

Corresponding author: G. Femenias (guillem.femenias@uib.es)

This work was supported in part by MINECO (Spanish Government) and FEDER through the project ELISA under Grant TEC2014-59255-C3-2-R), and in part by the Conselleria d'Educació, Cultura i Universitats (Govern de les Illes Balears) under Grant FPI/1538/2013 (co-financed by the European Social Fund).

ABSTRACT Two-tier networks combining an operator-managed infrastructure of macrocell base stations combined with a user-deployed network of femtocells have recently emerged in the context of modern wireless standards as a solution to meet the ambitious performance requirements envisaged in 4G/5G architectures. Most often, these systems require interference coordination schemes that allow near universal frequency reuse while maintaining a considerably high signal-to-interference-plus-noise ratio levels across the coverage area. In particular, fractional frequency reuse (FFR) and its variants are deemed to play a fundamental role in the next generation of cellular systems. This paper develops an analytical framework targeting the downlink performance evaluation of FFR-aided orthogonal frequency division multiple access-based two-tier heterogeneous networks. In the considered scenario, macrocell and femtocell tiers are assumed to be uncoordinated and co-channel deployed, thus representing a worst-case scenario in terms of inter-tier interference. The proposed framework allows the evaluation of the impact produced by both inter- and co-tier interferences on the performance of either the macro-users (MUs) or the femto-users. Analytical results are used to optimize the FFR parameters as a function of, for example, the density of MUs per cell, the resource block scheduling policy, the density of femto base stations per area unit, or the degree of isolation provided by wall penetration losses. Moreover, different optimization designs of the FFR component are proposed that allow a tradeoff between throughput performance and fairness by suitably dimensioning the FFR inner and outer areas and the corresponding frequency allocation.

INDEX TERMS Heterogeneous networks, femtocells, OFDMA, fractional frequency-reuse, optimization.

I. INTRODUCTION

A. MOTIVATION

The last breed of cellular communications standards such as the Long-Term Evolution (LTE) and LTE-Advanced (LTE-A) rely on the use of orthogonal frequency division multiple access (OFDMA) as the air-interface technology [1] and there are good chances that OFDMA will still play a key role in future 5G systems [2]. In OFDMA networks, the orthogonal time/frequency resources are organized into multiple resource blocks (RBs) that, based on predesigned frequency reuse plans, are distributed among cells. These RBs are then assigned to different users following predefined scheduling policies. Since RBs are allocated exclusively to one user per cell, intra-cell interference is eliminated completely. However, due to the common use of *aggressive* high spectral efficiency universal frequency reuse plans, OFDMA-based networks are greatly affected by high levels of inter-cell interference (ICI), harming particularly the users located in the cell-edge areas. In order to mitigate the ICI experienced by the cell-edge users while still achieving high spectral efficiencies, many different inter-cell interference control (ICIC) techniques have been proposed [3], among which *static* fractional frequency reuse (FFR) and all its variants have emerged as efficient ICIC techniques result in a good trade-off among the provision of high spectral efficiency, implementation complexity and cell-edge throughput enhancement [4], [5].

Aiming at even higher area spectral efficiencies, modern cellular systems are transitioning from planned

homogeneous (one-tier) macro-cellular networks to highly heterogeneous (multi-tier) deployments where consciously designed macro-cellular networks coexist with networks of femtocells installed by the end users that have the potential to offload traffic from the macrocells while providing high-quality low-cost network access to indoor users [6]. In these networks, due to the large cost of licensed spectrum, operators typically choose to allocate the same frequency bands to both macrocells and femtocells. As a result, these co-channel deployments result in what is usually known as inter-tier interference (ITI), which is particularly damaging for the femtocell users (FUs) connected to a femto base station (FBS) situated close to a macro base station (MBS) or the macrocell users (MUs) far from the MBS who are roaming in the vicinity of an FBS [7].

B. RELATED WORK

Previous works have focused on the simulation-based performance evaluation of two-tier macro/femto networks considering selected scenarios [8]–[10]. Simulation-based approaches, however, besides relying on computationally intensive, time-consuming, and proprietary system-level simulators, do not serve to capture the joint interplay of system design parameters and to infer theoretical insights behind the obtained performance results. This necessitates the development of accurate yet tractable analytical performance evaluation models. The analytical performance evaluation of multi-tier heterogeneous networks (HetNets) has been approached in recent years using stochastic geometry, where both MBSs and FBSs are distributed according to Poisson Point Processes (PPPs) (see, for instance, [11]–[13] and references therein). While stochastic geometry-based analyses lead to intuitive closed-form analytical solutions, in general, they evaluate the system performance by spatially averaging over all possible network realizations, including those that would never be considered in planned macrocellular set-ups. Using spatial averaging allows characterizing the performance for an entire network but, unfortunately, it does not allow the performance of a given cell to be accurately analysed. Note that this is an important metric for network designers interested in calculating the performance obtained over a given spatial region in the coverage area of the network. In trying to overcome some of the limitations of the stochastic geometry approach, Heath *et al.* [14] inscribed a circular cell within the weighted Voronoi cell provided by the PPP-based model in order to derive an upper bound to model the interference. Nevertheless, characterizing the MBS layouts using stochastic geometry makes it extremely difficult, if at all possible, to accurately capture the effects of using powerful ICIC techniques such as FFR and its variants and/or MBS cooperation schemes. We note that [15] and [16] do indeed tackle the performance analysis of FFR-based networks within the context of stochastic geometry, and despite the valuable insight their analyses provide at a network level, the proposed framework cannot be particularized to assess the performance at a specific cell level.

Unlike the aforementioned works, which rely on stochastic geometry to characterize both macrocell and femtocell tiers, Jin *et al.* [17] considered an FFR-aided twin-layer OFDMA network where stochastic geometry was used to model the random deployment of femtocells, while the macrocells were overlaid on top of the femtocells following a regular tessellation. One of the main contributions of [17] was the proposal of a spectrum swapping allocation for the femtocells, however, in order to prove the superiority of this spectrum sharing strategy in front of the classical full-spectrum reuse, some simplifications were introduced in the analytical framework, in particular: (i) indoor users were always linked to FBSs whereas outdoor users were always connected to MBSs, (ii) the small scale fading effects were not fully considered and, therefore, (iii) the performance analysis was restricted to resource allocation schemes adhering to the round robin scheduling policy. Similar approaches, lacking the full consideration of small scale fading and scheduling policies, were proposed by Assaad in [18] and Najjar *et al.* in [19] to optimize FFR-based parameters in a single-tier network. These limitations were overcome in part by Xu *et al.* in [20] (see also [21]) and [22], but only in the context of single-tier networks.

C. CONTRIBUTIONS OF THE PAPER

This paper presents an analytical framework allowing the performance evaluation of an FFR-aided OFDMA-based two-tier HetNet. A worst-case scenario in terms of inter-tier interference is evaluated in which macrocell and femtocell tiers are assumed to be uncoordinated and employ a co-channel deployment (full spectrum reuse); work dealing with spectrum sharing strategies can be found in, among many others, [23]–[25]. The main contributions of this paper can be summarized as follows:

- The first tier of the proposed framework comprises a planned FFR-based macro-cellular network modelled as a regular tessellation of hexagonally-shaped cells overlaying a randomly deployed second tier of low-power, low-complexity, short range femtocells. Such an approach can then be regarded as a hybrid model in between a deterministic two-tier deployment where the locations of all BSs are known *a priori*, and a stochastic two-tier deployment where both MBSs and FBSs are distributed using PPPs. As a major benefit of the hybrid approach proposed here, our model allows the analytical evaluation of two-tier HetNets that incorporate specific network parameters typically designed for planned macrocell networks (e.g., optimal threshold distance designs for different scheduling schemes in FFR-based OFDMA networks), while capturing the random nature of unplanned FBS deployments. Remarkably, the analytical model proposed in this paper allows the derivation of the average throughput provided by macro- or femto-BSs.
- Based on a unified approach, the analytical model allows the evaluation of the impact produced by the

inter- as well as the co-tier interferences on either the MUs or the FUs. The interference produced by the randomly allocated FBSs on either a reference MU or a reference FU is characterized by using the statistical distribution of the distance between two nodes whose positions adhere to a PPP distribution.

- Analytical results are used to optimize FFR-based parameters as a function of, for instance, the RB scheduling policy used in both tiers (e.g., round robin (RR) or maximum signal-to-interference-plus-noise ratio (MSINR)), the density of users per cell, the FBS density per area unit or the power attenuation due to wall penetration losses. The proposed optimization strategies aim at determining the size of the FFR-related spatial and frequency partitions maximizing the average macrocell throughput while at the same time fulfilling operator-defined restrictions such as using frequency partitions proportional to the area of the central and edge regions or attaining a prescribed fairness degree when allocating data-rates to the center and edge MUs. Unlike previous works, the proposed analytical framework is able to fully incorporate the effects of small-scale fading, thus allowing the optimization of the FFR parameters under different scheduling policies.

Although results are obtained for an FFR-aided macrocell deployment overlaid by a strict co-channel deployment of femtocells, the analytical framework proposed in this paper opens the door to the analytical performance of multi-tier OFDMA heterogeneous networks using more sophisticated ICIC techniques (e.g. soft frequency reuse, adaptive frequency reuse, network MIMO), other spectrum sharing strategies, and/or alternative RB scheduling algorithms. In particular, the resulting signal-to-interference-plus-noise ratio (SINR) expressions derived in this work could be used in conjunction with resource allocation algorithms [26], [27] to maximize some prescribed utility function. We note that a preliminary conference version of this work [28] was limited to uniform distributions of a fixed number of users per cell (i.e., PPP-based distributions were not taken into account) and furthermore, the analytical framework was not used to formulate optimization strategies aiming at improving the FFR-related system parameters.

D. PAPER ORGANIZATION

The rest of the paper is organized as follows. In Sections II and III, the system model under consideration is introduced alongside with the key simplifying assumptions made for the sake of analytical tractability of the proposed framework. Sections IV and V elaborate on the analytical frameworks used to characterize the overall macrocell and femtocell average throughput performance, respectively, according to both the MSINR and RR scheduling strategies. Optimal designs for the FFR-aided two-tier system are presented in Section VI. Extensive analytical and simulation results are provided in Section VII. Finally, the main outcomes of this paper are recapped in Section VIII.

II. SYSTEM MODEL

A two-tier (macrocell/femtocell) OFDMA cellular network providing service to a given set of mobile users is considered. Both the macrocell and femtocell tiers are co-channel deployed (i.e., they both use the same spectrum) with the femtocells operating under a closed-access policy.

MBSs are typically deployed following a well-planned strategy leading to a fairly regular distribution over the whole coverage area. Aiming at controlling the ICI in the macro-tier, the received average signal-to-interference-plus-noise ratio (SINR) is used to classify the different MUs as either cell-edge users, when the received average SINR is below a given threshold, or cell-centre users, when it is above that threshold. Non-overlapping frequency bands are then allocated to cell-center and cell-edge users, thus conforming to an static FFR scheme in which a frequency reuse factor equal to one is used for the cell-center users and a higher frequency reuse factor Δ (e.g., three or seven) is assumed for the cell-edge users. The complete system bandwidth consists of a set $\mathcal{F}_T$ of subcarriers, which is split into two subsets: the subset $\mathcal{F}_C$ of subcarriers allocated to the macrocell-center and the subset $\mathcal{F}_T \backslash \mathcal{F}_C$ of subcarriers allocated to the macrocell-edge. The subset $\mathcal{F}_T \backslash \mathcal{F}_C$ is further split into Δ equal parts $\mathcal{F}_{E1}$, ... and $\mathcal{F}_{E\Delta}$, of size $|\mathcal{F}_E|$, which are allocated to cell-edge MUs in such a way that adjacent cells will operate on different subsets of subcarriers.

A fraction of the coverage area is considered to be indoors (i.e., inside buildings), while the rest is outdoors. The femtocells are typically deployed by the owners in an unplanned manner within the indoor coverage area, thus only a fraction of the indoor area is covered by FBSs.

According to the previous system description, the base stations (BSs) can be classified into two tiers:

- **Tier 0**: MBSs, and
- **Tier 1**: FBSs.

Furthermore, the whole set of users, including femto-, macrocell-center and macrocell-edge users, can be classified as:

- **Class 0**: indoor FUs situated inside a building with femtocell coverage,
- **Class 1**: outdoor cell-center MUs,
- **Class 2**: indoor cell-center MUs situated inside a building with femtocell coverage,
- **Class 3**: indoor cell-center MUs situated inside a building without femtocell coverage,
- **Class 4**: outdoor cell-edge MUs,
- **Class 5**: indoor cell-edge MUs situated inside a building with femtocell coverage, and
- **Class 6**: indoor cell-edge MUs situated inside a building without femtocell coverage.

We note that this user classification generalizes the one proposed in [17] by allowing MUs to be outdoor or indoor.

A. CHANNEL MODEL

The downlink channel experiences small-scale fading as well as path loss including, potentially, wall penetration losses.[1] The path loss characterizing the link between a BS of tier t and a user of class s located at a distance of d (in meters) from the BS can be modeled as (in dB)

$$L_{t,s}(d) = K_{t,s} + 10\alpha_{t,s}\log_{10}(d), \tag{1}$$

where $K_{t,s}$ is a fixed path loss at a reference distance of one meter, and $\alpha_{t,s}$ is the path loss exponent. The main parameters and conditions of the path loss model used in this work have been drawn from [29] and are listed in Table 1. Notice that buildings have been characterized by a wall penetration loss W and thus, depending on the relative position of users with respect to the BSs, there are links that are not affected by any wall penetration loss (e.g., MBS-to-outdoor MU), links that are affected by a wall penetration loss W (e.g., MBS-to-indoor MU), and links that are affected by a two-wall penetration loss $2W$ (e.g., FBS-to-FU located in another femtocell) (see [29] for more details).

TABLE 1. Path loss model parameters.

Link	$K_{t,s}$	$\alpha_{t,s}$	Conditions
MBS - MU	15.3	3.76	$\forall d,\ t=0,\ s\in\{1,4\}$
	$15.3+W$	3.76	$\forall d,\ t=0,\ s\in\{2,3,5,6\}$
FBS - MU	$15.3+W$	3.76	$\forall d,\ t=0,\ s\in\{1,4\}$
	38.46	2	$d\leq 20$m, $t=0,\ s\in\{2,5\}$
	$15.3+2W$	3.76	$d>20$m, $t=0,\ s\in\{2,5\}$
	$15.3+2W$	3.76	$\forall d,\ t=0,\ s\in\{3,6\}$
MBS - FU	$15.3+W$	3.76	$\forall d,\ t=1,\ s=0$
FBS - FU	38.46	2	$d\leq 20$m, $t=1,\ s=0$
	$15.3+2W$	3.76	$d>20$m, $t=1,\ s=0$

III. ASSUMPTIONS AND PRELIMINARIES

A. ASSUMPTIONS

Assumption 1 (Circular Reference Macrocell): For the sake of analytical tractability, when obtaining the performance metrics for a particular MBS, termed the reference MBS, its coverage area will be approximated as a circle of radius R_m which, without loss of generality, will be chosen to match the area of the cell under consideration [20]. As an example, for the classical hexagonally-shapped regular tessellation shown in Fig. 1, the reference cell is approximated as a circle of radius $R_m = R_h\sqrt{3\sqrt{3}/(2\pi)}$, where R_h is used to denote the side of the regular hexagon.

Assumption 2 (Circular FFR-Defined Regions): Again, for analytical tractability, the reference macrocell-center and macrocell-edge regions will be separated by a circumference of radius R_{th} (threshold distance or threshold radius), as it can be appreciated in the example shown in Fig. 1 [17], [20].

[1]Note that in line with, among others, Xu *et al.* [20] and Jin *et al.* [17], and for the sake of analytical simplicity, shadowing is not considered in the proposed framework. Remarkably, it is contrasted by simulation in [20] that despite shadowing can affect the resulting throughput values, the optimum operational points (e.g., FFR optimum thresholds and spectrum allocation) do not significantly change with the inclusion of the shadowing component.

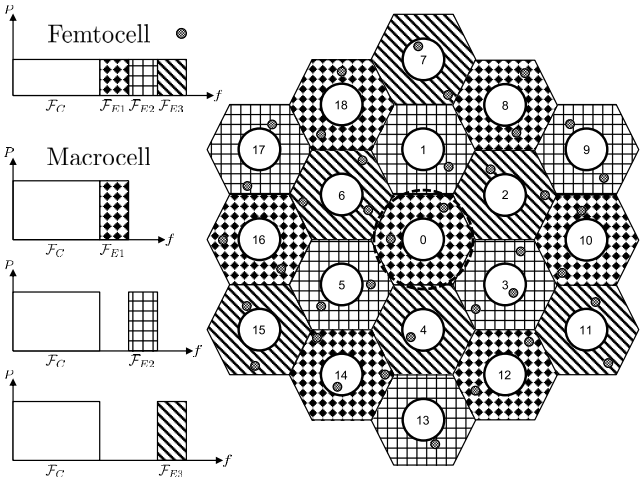

FIGURE 1. OFDMA-based and FFR-aided two-tier network topology.

Assumption 3 (Uniform Distribution of Buildings and FBSs): The buildings are assumed to be randomly located over the coverage area with each building having a certain probability of housing an active femtocell [17]. Femtocells are assumed to be non-overlapping and thus, the joint area of all femtocells can at most cover the whole indoor area of the system.

Assumption 4 (Circular Femtocells): Femtocells, as shown in the example network represented in Fig. 1, are modelled as small circular areas with radius R_f [17]. Assuming that femtocells are uniformly distributed with a normalized intensity of λ femtocells/m^2. For those buildings housing a femtocell, the FBSs, using omnidirectional antennas, are assumed to be located at the center of the femtocell.

Assumption 5 (Uniform distribution of MUs): Macro-users are independently and uniformly distributed with a normalized intensity λ_m (measured in users per area unit) over the service coverage area.

Assumption 6 (Uniform distribution of FUs within the femtocell): Femto-users connected to an active FBS are independently and uniformly distributed with a normalized intensity λ_f (measured in users per area unit) over the femto service coverage area.

A consequence of Assumptions 5 and 6 is that the probability distribution of the number $M_{\mathcal{S}}$ of users falling within the coverage area $A_{\mathcal{S}}$ of either an MBS or an FBS follows a Poisson distribution, thus implying

$$Pr\{M_{\mathcal{S}} = M\} = \frac{(\lambda_u A_{\mathcal{S}})^M e^{-\lambda_u A_{\mathcal{S}}}}{M!}, \tag{2}$$

with $\lambda_u = \lambda_m$ for the MUs and $\lambda_u = \lambda_f$ for the FUs.

B. SIGNAL-TO-INTERFERENCE-PLUS-NOISE RATIO

The instantaneous SINR experienced on the nth subcarrier by user u of class s served by BS b of tier t can be expressed as

$$\gamma_{b,t,u,s}[n] = \frac{P_t L_{t,s}(d_{b,t,u,s})\left|H_{b,t,u,s}[n]\right|^2}{N_0\Delta f + I_{b,t,u,s}[n]}, \tag{3}$$

where P_t denotes the per-subcarrier transmit power of any BS in tier t, $H_{b,t,u,s}[n] \sim \mathcal{CN}(0,1)$ is the frequency response resulting from the small-scale fading channel linking the BS b of tier t to user u of class s on the nth subcarrier, N_0 denotes the noise power spectral density, Δf is the subchannel bandwidth, and $I_{b,t,u,s}[n]$ denotes the interference term, which is given by

$$I_{b,t,u,s}[n] = \sum_{t' \in \{0,1\}} P_{t'} \sum_{b' \in \mathcal{B}_{b,t',u,s}[n]} L_{t',s}(d_{b',t',u,s}) \left| H_{b',t',u,s}[n] \right|^2, \quad (4)$$

with $\mathcal{B}_{b,t',u,s}[n] \subseteq \mathcal{B}_{t'}$ denoting the set of BSs of tier t' interfering user u of class s on subcarrier n. Obviously, the elements of the interfering sets are likely to differ for different classes of users and for different subcarriers. For instance, the set of interfering FBSs for a MU u of any class $s \in \{1, \ldots, 6\}$ and on any subcarrier n is $\mathcal{B}_{b,1,u,s}[n] = \mathcal{B}_1$, while the set of interfering FBSs for FU u served by FBS b on any subcarrier n is $\mathcal{B}_{b,1,u,0}[n] = \mathcal{B}_1 \backslash b$. Furthermore, for a cell-center MU u (classes $s \in \{1, 2, 3\}$) served by MBS b or a FU u (class $s = 0$) using cell-center subcarrier n, the set of interfering MBSs is $\mathcal{B}_{b,0,u,s}[n] = \mathcal{B}_0 \backslash b$ or $\mathcal{B}_{b,0,u,0}[n] = \mathcal{B}_0$, respectively. In contrast, for a cell-edge MU u (classes $s \in \{4, 5, 6\}$) served by MBS b or a FU u (class $s = 0$) using cell-edge subcarrier n, the set of interfering MBSs $\mathcal{B}_{b,0,u,s}[n]$ contains the indexes of all the MBSs using subcarrier n to serve cell-edge, except the reference MBS b in the former case.

Theorem 1 (Statistical Distribution of the SINR): When conditioned to the distances from user u of class s to both the serving BS b of tier t and the set of interfering BSs in subsets $\mathcal{B}_{b,0,u,s}[n]$ and $\mathcal{B}_{b,1,u,s}[n]$, the cumulative distribution function (CDF) of the instantaneous SINR $\gamma_{b,t,u,s}[n]$ in (3) can be expressed as

$$F_{\gamma_{b,t,u,s}[n] | \boldsymbol{d}_{b,t,u,s}}(x|\boldsymbol{d}) = 1 - \exp\left(-\frac{xN_0\Delta f}{\overline{P}_{b,t,u,s}}\right) \times \prod_{t' \in \{0,1\}} \prod_{b' \in \mathcal{B}_{b,t',u,s}[n]} \frac{1}{1 + x\frac{\overline{P}_{b',t',u,s}}{\overline{P}_{b,t,u,s}}}, \quad x \geq 0, \quad (5)$$

where $\boldsymbol{d}_{b,t,u,s}$ is a vector containing the distances from user u of class s served by BS b of tier t to all BSs contributing to its SINR, and $\overline{P}_{b',t',u,s} \triangleq P_{t'} L_{t',s}(d_{b',t',u,s})$ is used to denote the average received power from BS b' of tier t'.

Proof: See Appendix A. ∎

C. STATISTICAL MODEL OF THE FEMTOCELL DISTRIBUTION

Since it is assumed that the distribution of femtocells within the coverage area of the network is uniform, calculations accounting for their random positions would make the analytical tractability of the proposed framework rather involved. This step can be simplified by following a similar approach to the one used by Mawira in [30], the set of independent and identically distributed (i.i.d.) random variables $\{d_{b',1,u,s}[n]\}_{\forall b' \in \mathcal{B}_{b,t,u,s}[n]}$ representing the distances from the interfering FBSs to a given user u of class s served by a BS b of tier t and using subcarrier n, are first converted into the ordered set $\{d_{u,s}^{(b')}[n]\}_{b'=1}^{|\mathcal{B}_{b,t,u,s}[n]|}$, where $d_{u,s}^{(1)}[n] \leq d_{u,s}^{(2)}[n] \leq \ldots \leq d_{u,s}^{(|\mathcal{B}_{b,t,u,s}[n]|)}[n]$, and then the distance $d_{u,s}^{(j)}[n]$ to the jth nearest interfering FBS is approximated by $\mathbb{E}\{d_{u,s}^{(j)}[n] | d_{u,s}^{(1)}[n] \leq R_f\}$, when user u is located inside a building with femtocell coverage (i.e., MUs of classes $s \in \{2, 5\}$ as well as FUs), or by $\mathbb{E}\{d_{u,s}^{(j)}[n] | d_{u,s}^{(1)}[n] > R_f\}$, when user u does not have femtocell coverage (i.e., MUs of classes $s \in \{1, 3, 4, 6\}$), where $\mathbb{E}\{\cdot\}$ denotes the statistical expectation operation.

Theorem 2 (Expected Distances to Interfering FBSs): Given a uniform distribution of interfering FBSs with normalized intensity λ femtocells/m^2 around user u of class s using subcarrier n, the expected distance to the jth nearest interfering FBS when the user is located in a building with a circular femtocell coverage area of radius R_f can be expressed as

$$\mathbb{E}\left\{d_{u,s}^{(j)}[n] | d_{u,s}^{(1)}[n] \leq R_f\right\} = \begin{cases} \frac{R_f}{1-e^{\pi\lambda R_f^2}} - \frac{e^{\pi\lambda R_f^2}\,\mathrm{erf}\left(\sqrt{\pi\lambda}R_f\right)}{2\sqrt{\pi}(1-e^{\pi\lambda R_f^2})}, & j = 1 \\ \frac{\Gamma(j+1/2)}{\sqrt{\pi\lambda}\,(j-1)!\left(1-e^{-\pi\lambda R_f^2}\right)} - \frac{(\pi\lambda)^j R_f^{2j+1} e^{-\pi\lambda R_f^2} U\left(j, j+3/2, \pi\lambda R_f^2\right)}{1-e^{-\pi\lambda R_f^2}}, & j \geq 2, \end{cases} \quad (6)$$

where $\mathrm{erf}(\cdot)$ denotes the Gauss error function, $\Gamma(\cdot)$ is the Gamma function and $U(\cdot,\cdot,\cdot)$ is the confluent hypergeometric function of the second kind, also known as the Kummer's function of the second kind. In contrast, when the user is located outside areas with femtocell coverage, the expected distance to the jth nearest interfering FBS is given by

$$\mathbb{E}\left\{d_{u,s}^{(j)}[n] | d_{u,s}^{(1)}[n] > R_f\right\} = \begin{cases} R_f + \frac{e^{\pi\lambda R_f^2}\,\mathrm{erfc}\left(\sqrt{\pi\lambda}R_f\right)}{2\sqrt{\pi}}, & j = 1 \\ (\pi\lambda)^j R_f^{2j+1} U\left(j, j+3/2, \pi\lambda R_f^2\right), & j \geq 2, \end{cases} \quad (7)$$

where $\mathrm{erfc}(\cdot)$ is the Gauss complementary error function.

Proof: See Appendix B. ∎

IV. MACROCELL THROUGHPUT ANALYSIS

A. AVERAGE MACROCELL THROUGHPUT

Let us define $M_{\mathcal{S}_{b,0}}$ as a positive integer random variable representing the number of MUs in the region covered by the reference MBS b. Using this definition, the average throughput of the reference macrocell can be expressed as

$$\eta_{b,0} = \sum_{k=1}^{\infty} Pr\{M_{\mathcal{S}_{b,0}} = k\} \sum_{k_C=0}^{k} \binom{k}{k_C} P_C^{k_C} (1-P_C)^{k-k_C} \times \left[|\mathcal{F}_C| \eta_{b,0}^C(k_C) + |\mathcal{F}_E| \eta_{b,0}^E(k-k_C)\right], \quad (8)$$

where P_C denotes the probability that a MU is located in the reference cell-center region and $\eta^A_{b,0}(k_A)$ is the average macrocell throughput on a generic subcarrier allocated to cell-region A when there are k_A MUs in this region, where A is a token representing either the macrocell-center region C or the macrocell-edge region E.

Taking into account Assumptions 1, 2 and 5, the probability that a MU is located in the reference cell-center area is

$$P_C = \frac{R_{th}^2 - R_{0m}^2}{R_m^2 - R_{0m}^2}, \tag{9}$$

where R_{0m} denotes the minimum distance of a MU from its serving MBS. Now, defining M_A as a non-negative integer random variable representing the number of MUs in the cell region A covered by the reference BS, the average macrocell throughput on the nth subcarrier, allocated to macrocell region A when $M_A = k$, can be obtained as

$$\begin{aligned}\eta^A_{b,0}(k) &= \mathbb{E}_{\gamma^A_{b,0}|M_A}\left\{\Delta f \log_2(1+\gamma^A_{b,0})|M_A = k\right\} \\ &= \Delta f \log_2 e \int_0^\infty \frac{1 - F_{\gamma^A_{b,0}|M_A}(x|k)}{1+x}\,\mathrm{d}x,\end{aligned} \tag{10}$$

where $\gamma^A_{b,0}$ denotes the instantaneous SINR experienced on a generic subcarrier allocated to region A of macrocell b, and $F_{\gamma^A_{b,0}|M_A}(x|k)$ is its cumulative distribution function (CDF).

To arrive at closed-form expressions for the throughput, the CDF $F_{\gamma^A_{b,0}|M_A}(x|k)$ needs to be determined, which is strongly tied to the particular scheduling policy applied at the MBS.

B. MACROCELL MSINR SCHEDULING

Multiuser diversity is maximized when employing MSINR scheduling. In this case, a given subcarrier in region A is assigned to the user experiencing the highest SINR on that particular subcarrier, thus,

$$\gamma^A_{b,0}[n] = \arg \max_{(u,s)\in\mathcal{M}^A_{b,0}} \{\gamma_{b,0,u,s}[n]\}, \tag{11}$$

where $\mathcal{M}^A_{b,0}$ is used to denote the set of M_A MUs in region A served by the reference MBS b. Consequently, as on each subcarrier n in region A the MUs of the same class s are statistically equivalent in terms of SINR, the conditional CDF in the right-hand side (RHS) term of (10) simplifies to

$$\begin{aligned}F^{\mathrm{MSINR}}_{\gamma^A_{b,0}|M_A}(x|k) &\triangleq Pr\left\{\gamma^A_{b,0}[n] \leqslant x|M_A = k\right\} \\ &= \sum_{\substack{\forall k_{s_1^A},k_{s_2^A},k_{s_3^A}\in\{0,\ldots,k\} \\ k_{s_1^A}+k_{s_2^A}+k_{s_3^A}=k}} \binom{k}{k_{s_1^A}, k_{s_2^A}, k_{s_3^A}} \\ &\quad \times \prod_{i=1}^{3}\left(\frac{P_{s_i^A}}{P_A}\right)^{k_{s_i^A}}\left[F_{\gamma_{b,0,s_i^A}}(x)\right]^{k_{s_i^A}},\end{aligned} \tag{12}$$

with $k_{s_i^A}$ denoting the number of MUs of class s_i^A, where $[s_1^C, s_2^C, s_3^C] = [1, 2, 3]$ and $[s_1^E, s_2^E, s_3^E] = [4, 5, 6]$. Furthermore, with a slight abuse of notation, γ_{n,s_i^A} is used to denote the instantaneous SINR experienced by a generic MU of class s_i^A served by the reference MBS b when being allocated any of the available subcarriers. The probability $P_{s_i^A}$ that a MU belongs to class s_i^A is found to be

$$\begin{aligned}P_{s_1^A} &= (1-P_I)P_A, \\ P_{s_2^A} &= P_F P_A, \\ P_{s_3^A} &= (P_I - P_F)P_A,\end{aligned} \tag{13}$$

where, thanks to Assumptions 3 and 4, the probability P_F that an indoor MU is located in a building with femtocell coverage can be obtained as

$$P_F = \pi\lambda R_f^2. \tag{14}$$

The conditional CDF in (12) depends on the CDF of γ_{n,s_i^A} that can be obtained as

$$F_{\gamma_{b,0,s_i^A}}(x) = \mathbb{E}_{\boldsymbol{d}}\left\{F_{\gamma_{b,0,u,s_i^A}[n]|\boldsymbol{d}_{b,0,u,s_i^A}}(x|\boldsymbol{d})\right\}. \tag{15}$$

Using Theorem 2, the random variables representing the distances from the MU under analysis to the whole set of interfering FBS are approximated by deterministic values that can be calculated using (6) or (7). Hence, the distances to the interfering FBSs can be eliminated from the set $\boldsymbol{d}_{b,0,u,s_i^A}$ when calculating the expectation in (15). Furthermore, the positions of all the MBSs in the system are known (i.e., they are deterministic) and consequently, setting the origin of the coordinate system on the position occupied by the reference MBS, the random variable $d_{b',0,u,s_i^A}$ representing the distance from the interfering MBS b' to user u of class s_i^A can be expressed in terms of the random variables $d_{b,0,u,s_i^A}$ and $\theta_{b,0,u,s_i^A}$, denoting the modulus and phase of the polar coordinates of the MU under consideration with respect to the reference BS. Moreover, since MUs are uniformly distributed over the macrocell area, the random variables $d_{b,0,u,s_i^A}$ and $\theta_{b,0,u,s_i^A}$ are independent from each other and thus, summarizing, (15) can be rewritten as

$$\begin{aligned}&F_{\gamma_{b,0,s_i^A}}(x) \\ &\quad= \mathbb{E}_{d_{b,0,u,s_i^A},\theta_{b,0,u,s_i^A}}\left\{F_{\gamma_{b,0,u,s_i^A}[n]|d_{b,0,u,s_i^A},\theta_{b,0,u,s_i^A}}(x|d,\theta)\right\} \\ &\quad= \int_0^{2\pi}\int_{R_{\mathrm{L}}^A}^{R_{\mathrm{H}}^A} F_{\gamma_{b,0,u,s_i^A}[n]|d_{b,0,u,s_i^A},\theta_{b,0,u,s_i^A}}(x|d,\theta) \\ &\qquad\times f_{d_{b,0,u,s_i^A}}(d) f_{\theta_{b,0,u,s_i^A}}(\theta)\,\mathrm{d}d\,\mathrm{d}\theta,\end{aligned} \tag{16}$$

where the distances R_{L}^A and R_{H}^A are, respectively, the lower and higher radii of the circumferences delimiting macrocell region A, and $f_{d_{b,0,u,s_i^A}}(d)$ and $f_{\theta_{b,0,u,s_i^A}}(\theta)$ represent the PDFs of $d_{b,0,u,s_i^A}$ and $\theta_{b,0,u,s_i^A}$, that can be expressed as

$$f_{d_{b,0,u,s_i^A}}(d) = \begin{cases}\frac{2d}{(R_{\mathrm{H}}^A)^2-(R_{\mathrm{L}}^A)^2}, & R_{\mathrm{L}}^A \leq d \leq R_{\mathrm{H}}^A \\ 0, & \text{otherwise},\end{cases} \tag{17}$$

and

$$f_{\theta_{b,0,u,s_i^A}}(\theta) = \frac{1}{2\pi},\ 0 \le \theta \le 2\pi, \tag{18}$$

respectively. Furthermore, it is shown in [31] that the instantaneous SINR in multi-cell networks barely depends on the polar angle and thus,

$$F_{\gamma_{b,0,s_i^A}}(x) \simeq \frac{2}{(R_{\mathrm{H}}^A)^2 - (R_{\mathrm{L}}^A)^2} \times \int_{R_{\mathrm{L}}^A}^{R_{\mathrm{H}}^A} F_{\gamma_{b,0,u,s_i^A}[n]|d_{b,0,u,s_i^A}}(x|d) d \ \mathrm{d}d. \tag{19}$$

Note that this CDF characterizes the SINRs of all subcarriers and for all MUs of class s_i^A.

Finally, using (19), (12) and (10) in (8) and after some algebraic manipulations, the average macro-throughput of the FFR-aided OFDMA scheme in a two-tier network using MSINR follows

$$\eta_{b,0} = \eta_{b,0}^C + \eta_{b,0}^E, \tag{20}$$

where

$$\eta_{b,0}^A = \Delta f |\mathcal{F}_A| \log_2 e \times \int_0^\infty \frac{1 - e^{-\pi \lambda_m R_m^2 \left[P_A - \sum_{i=1}^3 P_{s_i^A} F_{\gamma_{b,0,s_i^A}}(x)\right]}}{1+x} \mathrm{d}x. \tag{21}$$

Computation of (21) can be easily tackled using numerical solvers such as those found in Mathematica or Matlab.

C. MACROCELL RR SCHEDULING

Given that the RR scheduler randomly allocates subcarriers to users and exploiting the fact that the user SINRs are statistically equivalent on each subcarrier, it is clear that serving $M_A = k$ users in macrocell-region A using RR amounts to serve $M_A = 1$ user by means of the MSINR [21]. Consequently

$$F^{\mathrm{RR}}_{\gamma_n^A|M_A}(x|k) = F^{\mathrm{MSINR}}_{\gamma_n^A|M_A}(x|1) = \sum_{i=1}^3 \frac{P_{s_i^A}}{P_A} F_{\gamma_{n,s_i^A}}(x). \tag{22}$$

Hence, using (19), (22) and (10) in (8) and after some algebraic manipulations, the average macrocell throughput of the FFR-aided OFDMA scheme in a two-tier network using the RR scheduling rule can be written as in (20) with

$$\eta_{b,0}^A = 2\Delta f |\mathcal{F}_A| \log_2 e \frac{1 - e^{-\pi \lambda_m R_m^2 P_A}}{(R_{\mathrm{H}}^A)^2 - (R_{\mathrm{L}}^A)^2} \sum_{i=1}^3 \frac{P_{s_i^A}}{P_A} \times \int_{R_{\mathrm{L}}^A}^{R_{\mathrm{H}}^A} \int_0^\infty \frac{\left[1 - F_{\gamma_{b,0,u,s_i^A}[n]|d_{b,0,u,s_i^A}}(x|d)\right] d}{1+x} \mathrm{d}x \ \mathrm{d}d. \tag{23}$$

V. FEMTOCELL THROUGHPUT ANALYSIS

A. OVERALL FEMTOCELL THROUGHPUT

The average throughput of a reference femtocell b can be obtained as

$$\eta_{b,1} = \sum_{k=1}^\infty Pr\{M_{\mathcal{S}_{b,1}} = k\} \left[\eta_{b,1}^C(k) + \sum_{i=1}^\Delta \eta_{b,1}^{Ei}(k)\right], \tag{24}$$

where $M_{\mathcal{S}_{b,1}}$ is a positive integer random variable representing the number of FUs in the region covered by FBS b and

$$\eta_{b,1}^S(k) = \Delta f \log_2 e \int_0^\infty \frac{1 - F_{\gamma_{b,1}^S|M_{\mathcal{S}_{b,1}}}(x|k)}{1+x} \mathrm{d}x, \tag{25}$$

with $\gamma_{b,1}^S$ denoting the instantaneous SINR experienced on a generic subcarrier that, in the macro-tier, has been allocated to cell-region S. The token S can represent either the macrocell-center region C, when dealing with subcarriers in $\mathcal{F}_C$, or any of the macrocell-edge regions Ei, when dealing with subcarriers in $\mathcal{F}_{Ei}$.

B. FEMTOCELL MSINR SCHEDULING

In an FBS implementing the MSINR scheduling rule, subcarrier n is allocated to the FU experiencing the highest instantaneous SINR on this subcarier. Hence,

$$\gamma_{b,1}[n] = \arg \max_{u \in \mathcal{M}_{b,1}} \left\{\gamma_{b,1,u,0}[n]\right\}, \tag{26}$$

where $\mathcal{M}_{b,1}$ is the set of $M_{\mathcal{S}_{b,1}}$ FUs served by reference FBS b. Setting, again, the origin of the coordinate system on the position occupied by the reference FBS and taking into account similar assumptions to those used in Subsection IV-B, the conditional CDF of $\gamma_{b,1}^S$ can be expressed as

$$F^{\mathrm{MSINR}}_{\gamma_{b,1}^S|M_{\mathcal{S}_{b,1}}}(x|k) = \left[F_{\gamma_{b,1,u,0[n]|d_{b,1,u,0}}}(x|d)\right]^k = \left[\frac{2}{(R_f^2 - R_{0f}^2)} \int_{R_{0f}}^{R_f} F_{\gamma_{b,1,u,0}[n]|d_{b,1,u,0}}(x|d) d \ \mathrm{d}d\right]^k, \tag{27}$$

for a generic subcarrier $n \in \mathcal{F}_S$ and with R_{0f} denoting the minimum distance of a FU from its serving FBS.

The average femtocell throughput using the MSINR scheduling rule can be obtained using (27) and (25) in (24) as

$$\eta_{b,1} = \eta_{b,1}^C + \sum_{i=1}^\Delta \eta_{b,1}^{Ei}, \tag{28}$$

where, after some algebraic manipulations,

$$\eta_{b,1}^S = \Delta f |\mathcal{F}_S| \log_2 e \times \int_0^\infty \frac{1 - e^{-\pi \lambda_f R_f^2 \left[1 - \frac{2\int_{R_{0f}}^{R_f} F_{\gamma_n^S|d_o,d_{fu}}(x|z,y) y \ \mathrm{d}y}{R_f^2 - R_{0f}^2}\right]}}{1+x} \mathrm{d}x. \tag{29}$$

C. FEMTOCELL RR SCHEDULING

As serving $M_{\mathcal{S}_{b,1}} = k$ FUs in a femtocell using RR is equivalent to serving one FU with MSINR, the conditional CDF of $\gamma^S_{b,1}$ conditioned on $M_{\mathcal{S}_{b,1}}$ can be obtained using (27) with $M_{\mathcal{S}_{b,1}} = 1$ as $F^{\text{RR}}_{\gamma^S_{b,1}|M_{\mathcal{S}_{b,1}}}(x|k) = F^{\text{MSINR}}_{\gamma^S_{b,1}|M_{\mathcal{S}_{b,1}}}(x|1)$. Therefore, the average femtocell throughput when using the RR scheduler can be obtained as in (28) where, in this case,

$$\eta^S_{b,1} = 2\Delta f\,|\mathcal{F}_S|\log_2 e\,\frac{1-e^{-\pi\lambda_f R_f^2}}{R_f^2 - R_{0f}^2} \times \int_{R_{0f}}^{R_f}\int_0^\infty y\,\frac{1-F_{\gamma^S_n|d_o,d_{fu}}(x|z,y)}{1+x}\,\mathrm{d}x\mathrm{d}y. \quad (30)$$

VI. OPTIMAL DESIGNS

This sections introduces a variety of designs targeting the optimization of FFR-aided two-tier OFDMA networks. Broadly speaking, these designs aim at dimensioning the FFR-related spatial and frequency partitions so that the average macrocell throughput is maximized while operator-defined constraints are fulfilled. Examples of such constraints are the use of area-proportional frequency partitions or the provision of fairness among the cell-center and cell-edge MUs. In particular, three FFR-based two-tier designs are explored: 1) Fixed-spectrum-allocation-factor Design (FxD), 2) Area-proportional Design (ApD) and 3) Quality-constrained Design (QoScD). With the first design, the use of a fixed frequency partition typically provides high spectral efficiencies at the cost of loosing fairness when allocating data rates to cell-center and cell-edge MUs. Using an area-proportional design allows a more equitable distribution of the spectrum that results in a higher degree of fairness between cell-center and cell-edge MUs, at the cost of reducing the average macrocell throughput with respect to the fixed-spectrum-allocation-factor design. To guarantee a certain degree of fairness between central and edge users, the optimization problem can be constrained to ensure that the cell-edge throughput is at least a fraction of the one achieved at the cell-center, in this way a certain quality of service (QoS) to the cell-edge MUs is provided while maximising the area spectral efficiency.

The parameters that will be used in posing the optimization problems are the spectrum allocation factor $\rho \triangleq |\mathcal{F}_C|/|\mathcal{F}_T|$ and the distance threshold ratio $\omega \triangleq R_{th}/R_m$. Expectably, the selection of these parameters greatly affects the average macrocell throughput per subchannel [17] that, for convenience, is defined as[2]

$$\tau(\omega,\rho) \triangleq \frac{\eta(\omega,\rho)}{\Delta f|\mathcal{F}_T|} = \rho\tau^C(\omega,\rho) + \frac{1-\rho}{3}\tau^E(\omega,\rho), \quad (31)$$

measured in bps/Hz/subchannel, where $\tau^A(\omega,\rho) \triangleq \frac{\eta^A(\omega,\rho)}{\Delta f|\mathcal{F}_A|}$ is the average throughput per subchannel in cell region A.

[2]Note that to emphasise its dependence on the optimization parameters ρ and ω, the overall average throughput is represented as $\eta(\omega,\rho)$.

A. FIXED-SPECTRUM-ALLOCATION-FACTOR DESIGN

Under FxD, the spectrum allocation factor is fixed to $\rho = \rho_o$ (typically $\rho_o = 0.5$). Therefore, only the parameter ω remains to be optimized and the problem can be formulated as

$$\omega^* = \arg\max_{0\le\omega\le1} \rho_o\tau^C(\omega,\rho_o) + \frac{1-\rho_o}{3}\tau^E(\omega,\rho_o). \quad (32)$$

B. AREA-PROPORTIONAL DESIGN

In this case, it is assumed that the MUs are uniformly distributed in the macrocell and that the number of subcarriers allocated to both the cell-center and the cell-edge MUs is proportional to the areas of both the cell-center and the-edge regions, respectively. That is, the so-called area-proportional ratio is used to determine the spectrum allocation factor as $\rho = \omega^2$ [17]. Based on this approach, the optimization problem can then be formulated as

$$\omega^* = \arg\max_{0\le\omega\le1} \omega^2\tau^C(\omega,\omega^2) + \frac{1-\omega^2}{3}\tau^E(\omega,\omega^2), \quad (33)$$

where, obviously, $\rho^* = \omega^{*2}$.

C. QoS-CONSTRAINED DESIGN

Trying to guarantee a certain degree of fairness between the cell-center and cell-edge MUs, the QoS-constrained design enforces that the per-subchannel average throughput allocated to a MU in the cell-edge region is at least a fraction q of the per-subchannel average throughput allocated to a MU in the cell-center region. Hence, in the QoScD approach the the FFR-related parameters are tuned establish a trade-off between the data rates allocated to the cell-center MUs and those allocated to the cell-edge MUs [17]. The corresponding constrained optimization problem can then be formulated in terms of the QoS factor q as

$$(\omega^*,\rho^*) = \arg\max_{0\le\omega,\rho\le1} \rho\tau^C(\omega,\rho) + \frac{1-\rho}{3}\tau^E(\omega,\rho), \quad \text{subject to } \tau^E_{mu}(\omega,\rho) \ge q\,\tau^C_{mu}(\omega,\rho), \quad (34)$$

where the implementation of different scheduling policies suggests the use of different definitions for the corresponding variables $\tau^A_{mu}(\omega,\rho)$. Let us assume that the number of MUs connected to the central MBS is $M_{\text{MBS}_0} = k$. In this case, as the main aim of the RR scheduling rule is to offer equitable access opportunities to the whole set of MUs, the per-MU and per-subchannel average macrocell throughput can be reasonably defined as $\tau^C_{mu}(\omega,\rho) = \frac{\rho\tau^C(\omega,\rho)}{P_C k}$ for the cell-center MUs and $\tau^E_{mu}(\omega,\rho) = \frac{(1-\rho)\tau^E(\omega,\rho)}{3(1-P_C)k}$ for the MUs located in the cell-edge region. In contrast, as the MSINR scheduling rule aims at providing service to the MU experiencing the highest instantaneous SINR, the definitions $\tau^C_{mu}(\omega,\rho) = \rho\tau^C(\omega,\rho)$ and $\tau^E_{mu}(\omega,\rho) = \frac{(1-\rho)\tau^E(\omega,\rho)}{3}$ seem to be more appropriate as, in this case, the average number of MUs in each of the cell regions is not taken into account when obtaining the corresponding per-subchannel average throughput values.

VII. NUMERICAL RESULTS

Aiming at validating the analytical framework proposed in previous sections and providing a set of practical design guidelines, the macro-tier is modelled as a cellular network with 19 MBs where the so-called macrocell of interest is surrounded by two interfering rings of MBSs (see Fig. 1). Without loss of generality, a frequency reuse $\Delta = 3$ is assumed in the cell-edge region of the FFR-aided scheme. The macro-tier is underlaid by a co-channel femto-tier that is modelled using a uniform random deployment of closed-access femtocells, that is, a deployment following a PPP distribution characterized by a normalized intensity λ (measured in FBSs per area unit). Furthermore, and as it has been stated in previous sections, PPPs of normalized intensities λ_m and λ_f (measured in users per area unit), are used to model the distribution of MUs and FUs over the corresponding coverage areas, respectively. Even though we have used the normalized intensities of the corresponding PPPs to develop the analytical framework described in previous sections, for the sake of presentation clarity, results shown in this section will be expressed as a function of the average number of FBSs per macrocell ($N_f \triangleq \pi\lambda R_m^2$), the average number of MUs per macrocell ($M \triangleq \pi\lambda_m R_m^2$) and the average number of FUs per femtocell ($M_f \triangleq \pi\lambda_f R_f^2$). The per-tier average spectral efficiency is evaluated for the OFDMA-based FFR-aided two-tier network under different system configurations and using the optimal designs described in Section VI. Based on [29], Table 2 summarizes the main system parameters that have been used to obtain both the simulated and analytical results.

TABLE 2. Network parameters.

System parameter	Value
Number of macrocells	19
Urbanization factor	0.6
Macrocell radius	500 m
Minimum distance between MBS and users	35 m
Femtocell radius	20 m
Minimum distance between FBS and users	0.2 m
Antenna configuration	SISO
Transmit power of the MBS	46 dBm
Antenna gain at the MBS	14 dBi
Transmit power of the FBS	20 dBm
Antenna gain at the FBS	5 dBi
Power spectral density of noise	-174 dBm/Hz
Receiver noise figure	7 dB
Total bandwidth	20 MHz
Total number of subcarriers	512
Reuse factor	3
Multi-path model	Rayleigh fading
Monte Carlo trials	10,000

A. FXD-BASED MACROCELL FFR

The average macrocell spectral efficiency (measured in bps/Hz) is shown in Fig. 2 for the fixed optimization design as a function of the distance threshold R_{th}. Aiming at illustrating the system behaviour under a wide variety of network deployments, simulation and analytical results are provided

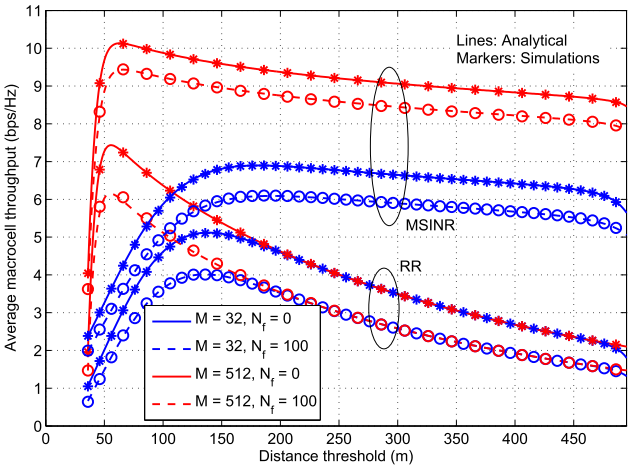

FIGURE 2. Average macrocell throughput versus distance threshold R_{th}, average number of MUs per macrocell M and FBS density N_f (FxD, $W = 10$ dB).

for both the RR and MSINR scheduling policies and using different combinations of the average numbers of FBSs and MUs per macrocell. The first obvious conclusion to be drawn from the observation of these results is that there is an almost perfect match between the results obtained using analysis (lines) and those obtained through Monte-Carlo simulations (markers) and, therefore, this validates the analytical framework developed in Section IV. Focusing now on performance issues, it can be observed that the effects of a dense femtocell deployment on the average macrocell throughput degradation are more pronounced when using the RR scheduler than when implementing the MSINR scheduling rule. As expected, due to the exploitation of the multiuser diversity, the average throughput provided by the MSINR scheduling rule increases with the average number of MUs per macrocell. Nonetheless, there is another effect, more apparent when using the RR scheduling rule, that produces also an increase of the average throughput with the number of MUs. Increasing the average number of MUs per macrocell increases both the probabilities of having at least one cell-edge MU and one cell-center MU, hence reducing the probability of wasting resources in those cases in which subcarriers cannot be allocated because the BS has no users to serve. Furthermore, note that increasing the average number of MUs per macrocell produces a decrease in the optimal distance threshold, thus reducing the size of the macrocell-center region and increasing the impact the average macrocell-edge throughput has on the average macrocell throughput. The decrease of the optimal value of R_{th} with the average number of MUs per macrocell can be appreciated for both the MSINR and RR scheduling rules.

Once the accuracy and precision of the proposed analytical framework has been established, and unless otherwise stated, we note that results shown next only depict the analytical results, notwithstanding all of them have been duly replicated by means of simulations. Using the wall penetration loss as parameter, Fig. 3 shows the degradation of the optimal macrocell throughput produced by an increase in the

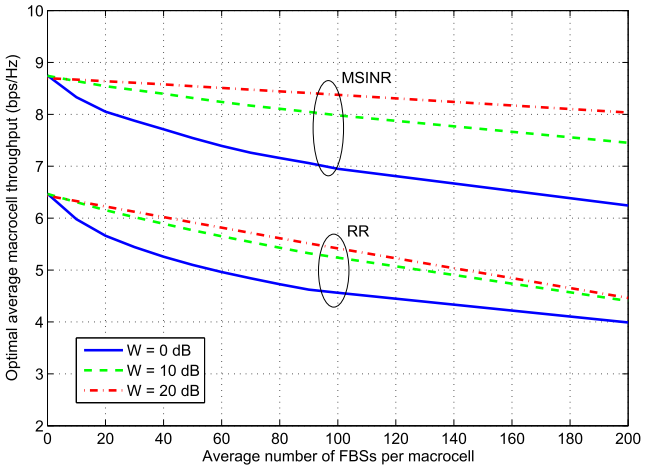

FIGURE 3. Optimal average macrocell throughput versus the average number of FBSs per macrocell N_f and wall penetration losses W (FxD, $M = 128$).

average number of FBSs per macrocell. When compared to the MSINR scheduling policy, a higher degradation slope can be appreciated when using the RR scheduler, specially for urban environments with buildings constructed with materials providing high levels of isolation (i.e., buildings with W ranging from 10 to 20 dB). This can be explained by the fact that the scheduled MUs are typically more robust against interference when using an MSINR scheduling rule than for the case of an RR scheduler.

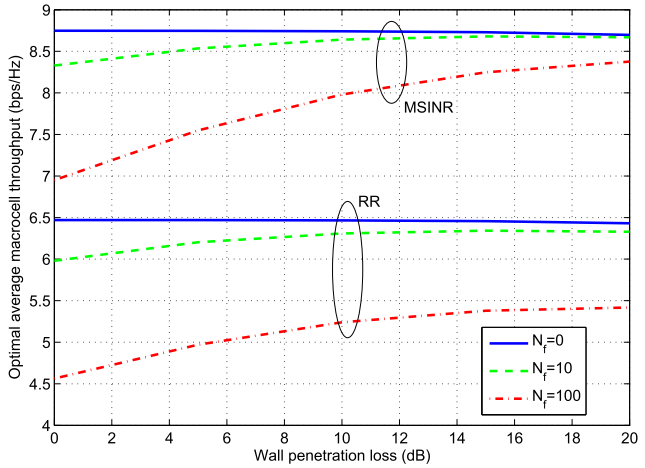

FIGURE 4. Optimal average macrocell throughput versus wall penetration loss W and FBS density N_f (FxD, $M = 128$).

Results presented in Fig. 4 compare the optimal macrocell throughput performance versus the wall penetration loss using the average number of FBSs per macrocell as a parameter. In the absence of the femtocell tier ($N_f = 0$), the optimal average macrocell throughput experiences a negligible degradation when increasing the wall penetration losses because, assuming that the thermal noise power is residual in front of the intercell interference, both the useful and the interfering signals for indoor MUs are affected by exactly the same attenuation factor. In contrast, in environments with a high FBS density, increasing the wall penetration losses produces an increase in the the average macrocell throughput because, in this case, high wall penetration losses protect indoor and outdoor MUs in front of cross-tier interference generated by neighboring FBSs.

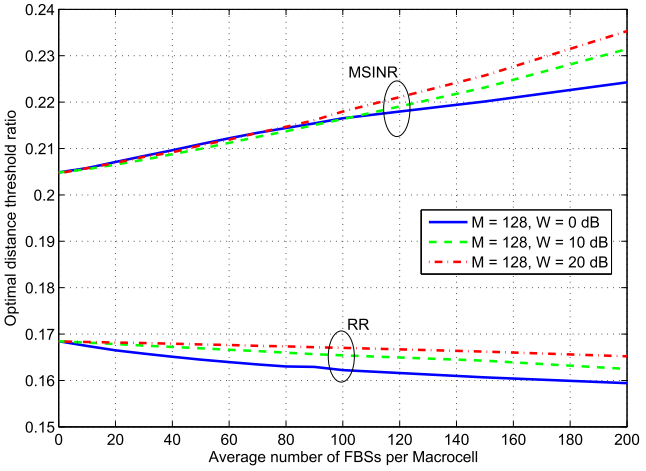

FIGURE 5. Optimal distance threshold ratio versus average number of FBSs per macrocell N_f and wall penetration losses W (FxD, $M = 128$).

The optimal distance threshold ratio versus the average number of FBSs per macrocell is shown in Fig. 5 for different values of the wall penetration loss and assuming, without loss of generality, an average number of MUs per macrocell $M = 128$. As it can be observed, using the MSINR scheduling rule results in a higher optimal distance threshold when compared with that obtained using the RR rule. This is because MUs in the cell-center region experience a much higher SINR than the cell-edge MUs and as the MSINR scheduler favours users with good channel conditions, the optimal fixed-spectrum-allocation-factor design for the MSINR rule results in larger cell-center areas. Another interesting effect is that increasing the average number of FBSs per macrocell produces an increase in the optimal distance threshold ratio in an MSINR-based system but, in contrast, it results in a decrease of this parameter when using an RR scheduling rule. These dissimilar behaviours can be explained by the fact that the femto-tier interference effects are less significant when affecting the best users selected by the MSINR scheduler, specially the best cell-center FUs, than when affecting a randomly selected user in an RR-based system. It is also interesting to consider the effect the wall penetration losses have on ω^* as N_f increases. Irrespective of the applied scheduling rule, increasing the wall penetration losses produces an increase of the optimal distance threshold ratio that is more apparent for high values of N_f. The rationale behind this behaviour can be found in the fact that increasing W results in a general decrease of the interference produced by the femto-tier, interference reduction that produces a higher throughput increase in those MUs close to the MBS, that is, those MUs likely to be cell-center users, thus leading to an expansion of the central region (increase of ω).

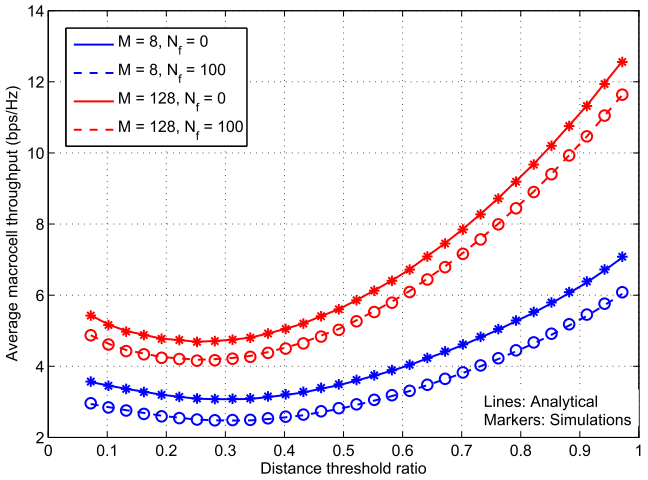

FIGURE 6. Average macrocell throughput versus distance threshold R_{th}, average number of MUs per macrocell M and FBS density N_f (ApD, MSINR, $W = 10$ dB).

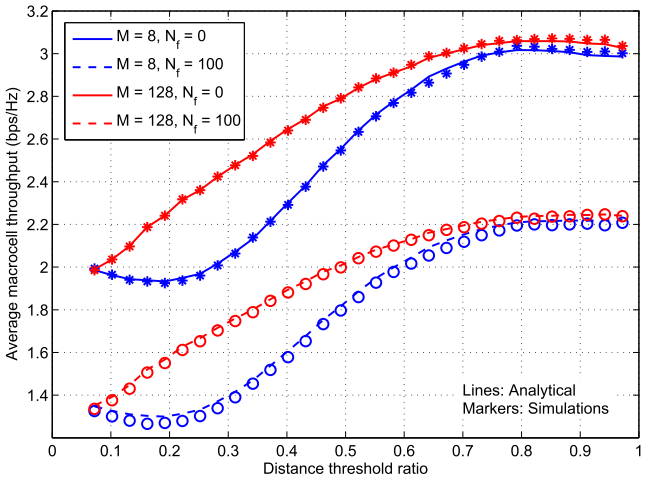

FIGURE 7. Average macrocell throughput versus distance threshold R_{th}, average number of MUs per macrocell M and FBS density N_f (ApD, RR, $W = 10$ dB).

B. ApD-BASED MACROCELL FFR

As it was stated in Section VI, macrocell FFR optimization problems based of area-proportional designs use an spectrum allocation factor $\rho = \omega^2$. Using this setup, the simulated and analytical average macrocell throughput as a function of the distance threshold ratio ω and with different configurations of number of FBSs and MUs per macrocell are shown in Figs. 6 and 7 for the MSINR and RR scheduling policies, respectively. As expected, as it does not make use of the multiuser diversity, the RR scheduler provides much lower average throughput figures than the MSINR scheduling rule. An effect that becomes more and more evident as the density of MUs per macrocell increases. The effects of increasing the density of FBSs per macrocell are similar to those observed in FxD-based macrocell FFR systems, with a more pronounced degradation of the average macrocell throughput when using the RR scheduler than for the MSINR scheduling rule.

As it can be observed in Fig. 6, when using an MSINR scheduling strategy in an ApD-based FFR-aided network, the optimal distance threshold ratio is $\omega^* = 1$ irrespective of the network configuration, thus implying that the optimal ApD spectral allocation factor is $\rho^* = 1$. That is, in an ApD-based FFR-aided network using an MSINR scheduler, the optimal solution consists in eliminating the cell-edge regions and allocating all the subcarriers to the cell-center area (i.e., the optimal solution consists in using a full spectrum reuse strategy). This can be explained by the fact that the MSINR scheduling rule does not provide fairness to the set of served users and thus, the optimal ApD allocates the available resources to MUs experiencing high SINR values, that is, MUs located in the cell-center.

Results are quite different when using the fairness-driven RR scheduling policy. In this case, and as it can be observed in Fig. 7, there is an optimal distance threshold ratio that is rather insensitive to the density of MUs per macrocell but tends to increase as the density of FBSs per macrocell increases. Furthermore, as the RR scheduling rule does not take advantage of the multiuser diversity, the optimal values of ω (and hence, those of ρ) are almost independent of M. The displacement of the optimal value of ω^* to higher values as the femtocell density increases can be explained by the fact that a given femto-tier interference power produces a higher effect on those MUs experiencing lower SNIRs (i.e., those MUs laying on the cell-edge region) and thus, the optimal design tends to favour cell-center MUs by allocating more resources to them.

C. QoScD-BASED MACROCELL FFR

The QoScD strategy allows setting different average throughput fairness requirements between cell-edge and cell-center MUs. Hence, in order to observe the system behaviour under high and low QoS constraints, quality factors of $q = 0.2$ and $q = 0.02$ will be considered, respectively. Using different configurations of the densities of MUs and FBSs per macrocell for both the RR and the MSINR scheduling policies, analytical and simulated average macrocell throughput results are shown in Fig. 8 as a function of the distance threshold ratio ω. Note that for the results shown in this figure, for each value of ω, the value of ρ maximising the average macrocell throughput has been used. Indeed, the pairs (ω, ρ) optimizing the average macrocell throughput observed in these graphs have been obtained by solving problem (34). Because of the exploitation of multiuser diversity, the MSINR scheduling policy shows a clear advantage in terms of average throughput performance when compared to the RR strategy. A performance advantage that, as in the FxD- and ApD-based schemes, becomes more pronounced in macrocell environments with a high density of MUs. Increasing the QoS requirement q enforces a higher degree of fairness between cell-center and cell-edge MUs at the cost of decreasing the spatially averaged macrocell throughput. Additionally, note that the average throughput degradation produced by the increase of the density of FBSs per macrocell is more obvious

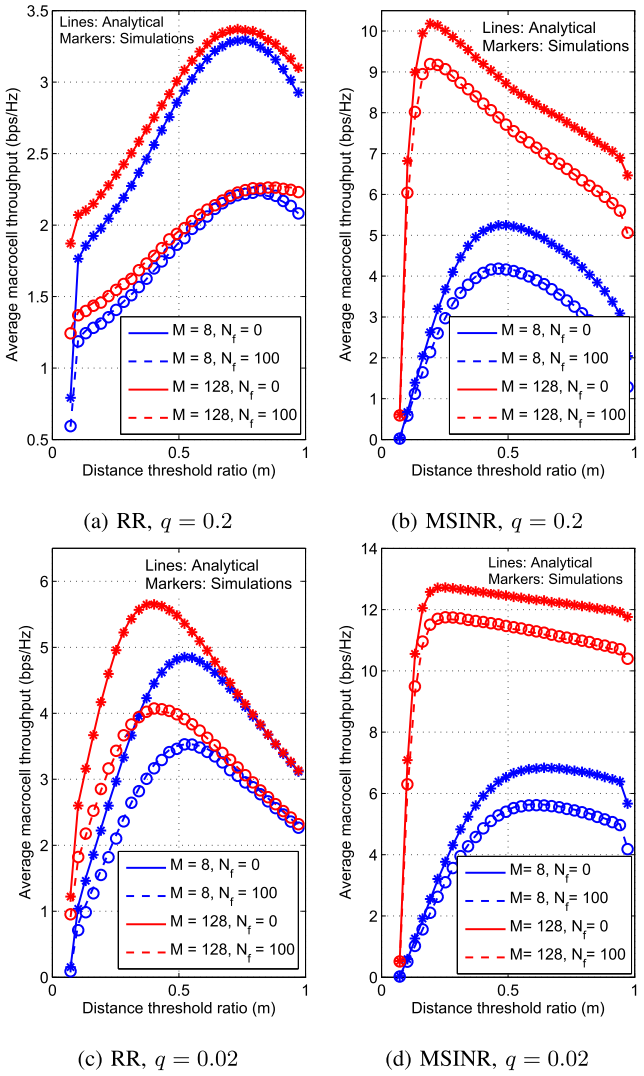

(a) RR, $q = 0.2$ (b) MSINR, $q = 0.2$

(c) RR, $q = 0.02$ (d) MSINR, $q = 0.02$

FIGURE 8. Average macrocell throughput versus distance threshold R_{th} (assuming the use of the corresponding optimal value of ρ), average number of MUs per macrocell M and FBS density N_f (QoScD, $W = 10$ dB). (a) RR, $q = 0.2$. (b) MSINR, $q = 0.2$. (c) RR, $q = 0.02$. (d) MSINR, $q = 0.02$.

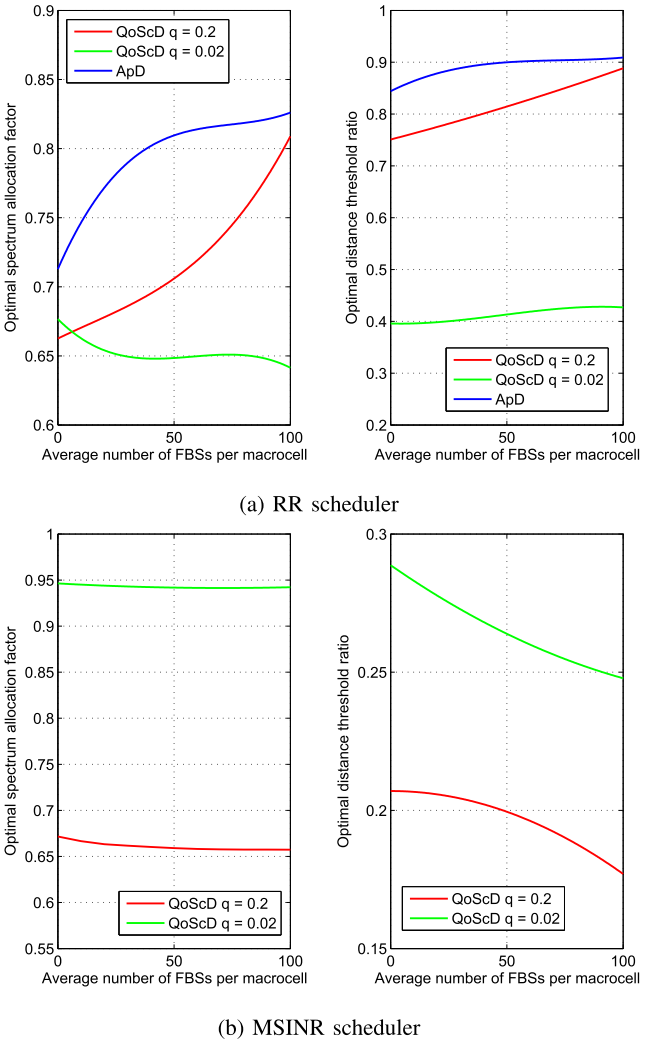

(a) RR scheduler

(b) MSINR scheduler

FIGURE 9. Optimal spectrum allocation factor ρ^* and distance threshold ratio ω^* versus the average number of FBSs per macrocell N_f and the QoS requirement q (QoScD/ApD, $M = 128$, $W = 10$ dB). (a) RR scheduler. (b) MSINR scheduler.

for the RR scheduling policy than for the MSINR scheduler, specially for the case of a quality factor $q = 0.02$.

As it can be observed in Figs. 8 and 9, when using the RR scheduling rule both the optimal distance threshold ratio and the optimal spectrum allocation factor increase with the quality factor q at the expense of a reduction in the average macrocell throughput.[3] In fact, recalling that $\tau^A_{mu}(\omega, \rho)$ is defined as the average per-subcarrier and per-MU throughput in region A and that the q is defined as the requirement that $\tau^E_{mu}(\omega, \rho)$ is greater than a certain fraction of $\tau^C_{mu}(\omega, \rho)$, strict QoS constraints in an RR-based network can only be fulfilled by increasing both the cell-center area (i.e., the number of cell-center MUs) and the number of subcarriers allocated to the cell-center MUs. Interference increase produced by the femto-tier densification produces a clear increase of ω^* and a not so obvious behaviour of ρ^* that increases for $q = 0.2$ and decreases for $q = 0.02$. In fact, both the objective function and the constraint in problem (34) show a highly nonlinear dependence with respect to the optimization variables ω and ρ and this makes it very difficult to provide an intuitive explanation of its behaviour.

Full spectrum reuse has been found to be the one providing the maximum average macrocell throughput when assuming an ApD-based network under MSINR scheduling. This solution coincides with that obtained when designing a QoScD-based FFR-aided network with $q = 0$. Despite this is a trivial non-realistic QoS constrained design, it can help to understand the MSINR-related results in Figs. 8 and 9. Since a minimum degree of fairness between cell-edge and cell-center MUs is enforced by the QoScD strategy, the constrained design targeting the maximization of the average

[3]For comparison reasons, results for the area-proportional design are also provided in Fig. 9.

macrocell throughput may no longer match the full spectrum reuse scheme, however, note that the optimal spectrum allocation factor for $q = 0.02$ approaches 95% of all the available spectral resources, that is, the optimal design shows a clear tendency to the full spectrum reuse strategy. In fact, irrespective of the average number of FBSs per macrocell, increasing the QoS requirement from $q = 0.02$ to $q = 0.2$ produces a notable decrease in both the optimal distance threshold ratio and the optimal spectrum allocation factor, thus increasing the amount of spatial and frequential resources allocated to the cell-edge MUs. The optimal spectrum allocation factor is rather insensitive to the femto-tier density. In contrast, increasing the average number of FBSs per macrocell results in a decrease of the optimal distance threshold ratio. That is, increasing the femto-tier interference affecting the MUs produces a decrease of the optimal cell-center area. This is because increasing the femto-tier interference harms more the cell-edge MUs than the cell-center MUs and the QoScD, in order to continue fulfilling the constraint in problem (34), is bound to decrease the optimal threshold radius.

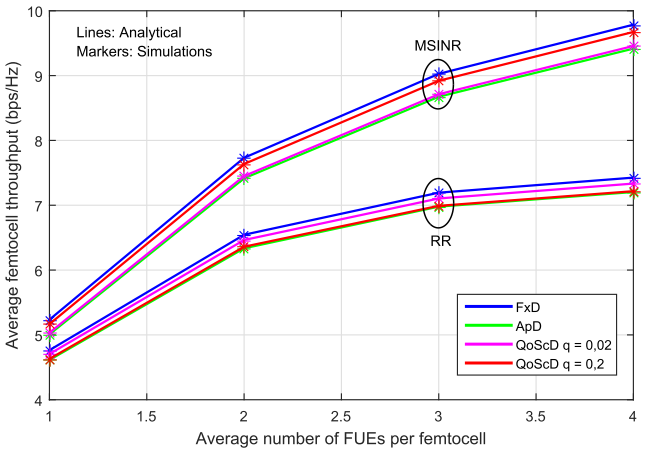

FIGURE 10. Average femtocell throughput versus the average numbers of FUs per femtocell and FFR-aided macrocell optimization design ($d_0 = 350$ m, $N_f = 100$ FBs/macrocell, $M = 128$ MUs/macrocell, $W = 10$ dB).

D. FEMTOCELL NETWORK

Considering now the performance evaluation of the femtocell tier, and assuming that the macro-tier uses the optimal ρ and ω for each particular set-up, Fig. 10 presents the average spectral efficiency for a reference femtocell as a function of the average number of FUs and for the different FFR-based macrocell designs, when using either an RR scheduling rule or an MSINR scheduler. Without loss of generality, the reference FBS is located at a distance $d_0 = 350$ meters from the central MBS, the average number of MUs per macrocell is fixed to $M = 128$, the wall penetration loss has been assumed to be $W = 10$ dB and the average number of FBSs per macrocell has been set to $N_f = 100$. As in the case of the macrocell network, note the very accurate match between analytical (lines) and simulation (markers) results, thus validating the analytical framework developed in Section V. It can be observed that increasing the average number of FUs in the reference femtocell leads to an improvement in its average throughput. This behavior is due to the lower probability of not having any FU attached to this femtocell, with the consequent waste of resources (i.e., a femtocell infrastructure providing service to nobody), and moreover, for the particular case of the MSINR scheduler, to the higher degree of multiuser diversity.

Inter-tier interference produced by different FFR-based macrocell designs results in different levels of degradation on the femto-tier basically due to the fact that the number of subcarriers allocated to the cell-center and cell-edge areas (i.e., the spectrum allocation factor ρ) is design-dependent. As the subcarriers allocated to the cell-edge MUs suffer from less macro-tier interference, the more subcarriers are allocated to the cell-edge (i.e., the less ρ is) the higher is the average throughput experienced in the femto-tier. As the optimal spectrum allocation factor of ApD and QoScD is higher than that used in the FxD (see Fig. 9), using FxD with $\rho = 0.5$ in the FFR-aided macro-tier provides the highest average femtocell throughput. As ApD is the one exhibiting the highest optimal spectrum allocation factor for both the RR and the MSINR schedulers, using ApD in the FFR-aided macro-tier produces the highest degradation in the average femtocell throughput. Degradation effects produced by the QoS constrained designs lie in between those produced by the fixed and area-proportional designs.

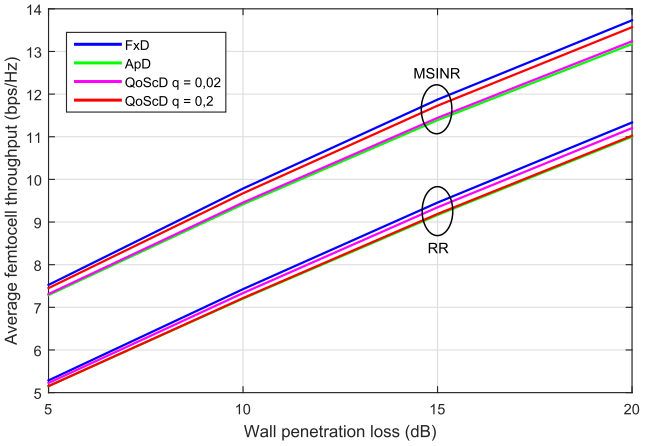

FIGURE 11. Average femtocell throughput versus wall penetration loss and FFR-aided macrocell optimization design ($d_0 = 350$ m, $N_f = 100$ FBs/macrocell, $M = 128$ MUs/macrocell, $M_f = 4$ FUs/femtocell).

In Fig. 11, assuming $M = 128$ MUs/macrocell, $N_f = 100$ FBSs/macrocell and an average number of FUs $M_f = 4$ served by the reference femtocell located at a distance $d_0 = 350$ meters from the central MBS, the average throughput for this particular FBS is shown as a function of the wall penetration losses for the different FFR-based macrocell designs and applying RR and MSINR scheduling policies. It can be seen how, irrespective of the applied FFR-aided macro-tier design, a large wall penetration loss

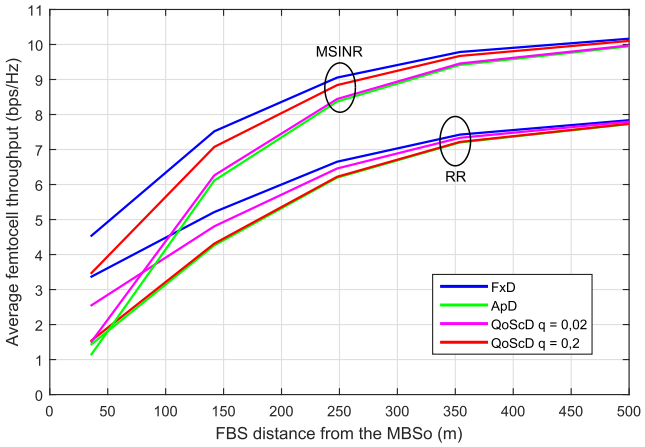

FIGURE 12. Average femtocell throughput versus distance to the nearest MBS and FFR-aided macrocell optimization design ($N_f = 100$ FBs/macrocell, $M = 128$ MUs/macrocell, $W = 10$ dB, $M_f = 4$ FUs/femtocell).

leads to a better femto-throughput performance because, in this case, the walls protect the *indoor* FUs from the interference emanating from both the macro- and femto-tiers. That is, wall penetration losses are always beneficial for the indoor FUs in terms of average spectral efficiency.

Finally, Fig. 12 depicts the average reference FBS throughput as a function of its distance to the central MBS (notice that this distance ranges from R_{0m} to R_m) for the different FFR-based macrocell designs and scheduling strategies. In this particular result, the system is parameterized with $M = 128$ MUs/macrocell, $W = 10$ dB, $N_f = 100$ FBSs/macrocell and $M_f = 4$ FUs attached to the reference FBS. Clearly, FBSs located far-away from a MBS achieve higher average throughput owing to a lower interference caused by the macro-tier. Note that for the majority of distances to the MBS, MSINR outperforms RR, however, when the reference FBS is located in the proximity of the MBS, for certain FFR-based macrocell designs (i.e., ApD and QoScD with $q = 0.02$) the RR scheduler provides an advantage over the MSINR scheduling rule. For these particular designs, and unlike in RR scheduling, the optimal value of ρ when applying MSINR scheduling is almost equal to one, that is, virtually all subcarriers are allocated to the center-region and thus, in the vicinity of the MBS, most of the subcarriers used by the FBS will be affected by a high level of inter-tier interference thus resulting in a decreased average femtocell throughput.

VIII. CONCLUSION

This paper has introduced an analytical framework to evaluate the performance of two-tier FFR-aided OFDMA networks that is able to incorporate the regular distribution of the macro base stations with randomly-deployed users and femto base stations adhering to Poisson-point processes. Monte Carlo simulations have been used to thoroughly validate the analytical results. Regarding the macro-tier, numerical results show that the macrocell throughput tends to increase when number of macro-users in the system grows, as the probability of having empty FFR-defined areas (i.e., cell-center or cell-edge without any user) vanishes, thus preventing radio resources assigned to each area from being wasted. Remarkably, when employing MSINR scheduling, the exploitation of multiuser diversity helps to further magnify the macrocell throughput improvement. Increasing the number of FBSs per macrocell rises the inter-tier interference, thus causing a significant degradation on the macrocell throughput, which has been found to be of comparable magnitude for both scheduling policies. Most of the effects observed in the macro layer are also mimicked at the femto level, where in this case the femto-tier performance degradation observed with an increased number of femtos is caused by an enhanced level of intra-tier interference. Multiuser diversity, as in the macro tier, is also observed to very significantly increase the femtocell throughput when using MSINR even for a small number of femto users. Remarkably, the optimal threshold radius in the FFR design, has been found to significantly depend on the number of FBSs per macrocell and the number of MUs per cell, thus clearly revealing the close relation between femto-network characteristics and the macrocell FFR component as well as the relevance of analytical frameworks, such as the one introduced here, that jointly consider both macro and femto tiers. Finally, a variety of FFR designs have been proposed by suitably dimensioning the edge and central FFR defined-regions and the corresponding amount of frequency resources assigned to each region. In particular, ApD and QoScD designs have been shown to offer different operating points in the throughput *vs* fairness plane. The proposed model also incorporates wall penetration losses. It has been found that the effects these losses have on the average femtocell throughput barely depend on the scheduling technique or FFR design, whereas when evaluating the average macrocell throughput, this has been shown to exhibit a clear dependence on the number of active femtocells.

Further work will progress along different lines. Firstly, by demonstrating how the proposed analysis can be tailored to more sophisticated ICIC techniques. Notice for instance that by allowing the FFR-defining thresholds to vary in time or by using different reuse patterns, the analytical performance of adaptive and soft frequency reuse schemes could be tackled, and that by relying on the SINR expressions achievable when using network MIMO schemes, combined cooperative and multi-tier networks could be analyzed. Secondly, more sophisticated scheduling techniques, such as proportional fair (PF), will be incorporated. Finally, other spectrum sharing strategies can be explored such as those based on the spectrum swapping technique mentioned in the Introduction.

APPENDIX A
PROOF OF THEOREM 1

In order to simplify notation, let us define the random variable γ representing the instantaneous SINR experienced by a generic user on a generic subcarrier. Let us also assume that

this SINR can be expressed as

$$\gamma = \frac{|x_0|^2}{N_0\Delta f + \sum_{i=1}^{r}|x_i|^2}, \tag{35}$$

with $\{x_i\}_{i=0}^{r}$ denoting a set of $r+1$ independent zero-mean complex-normal random variables with variance $\overline{P}_i$, for all $i \in \{0,\ldots,r\}$. In this case, when conditioned on the set of random variables $\{x_i\}_{i=1}^{r}$, the CDF of γ can be obtained as

$$\begin{aligned} &F_{\gamma|x_1,\ldots,x_r}(x|y_1,\ldots,y_r) \\ &\quad= \Pr\{\gamma \le x | x_1 = y_1,\ldots,x_r = y_r\} \\ &\quad= \Pr\left\{x_0 \le x\left(N_0\Delta f + \sum_{i=1}^{r} y_i\right)\right\} \\ &\quad= 1 - \exp\left(-x\frac{N_0\Delta f + \sum_{i=1}^{r} y_i}{\overline{P}_0}\right), \quad x \ge 0. \end{aligned} \tag{36}$$

Now, averaging over the PDFs of the random variables in the set $\{x_i\}_{i=1}^{r}$ yields

$$\begin{aligned} F_\gamma(x) &= \int_0^\infty \cdots \int_0^\infty F_{\gamma|x_1,\ldots,x_r}(x|y_1,\ldots,y_r) \\ &\quad \times f_{x_1}(y_1)\cdots f_{y_r}(y_r)\mathrm{d}y_1\cdots\mathrm{d}y_r \\ &= 1 - \exp\left(-x\frac{N_0\Delta f}{\overline{P}_0}\right)\prod_{i=1}^{r}\int_0^\infty \exp\left(-x\frac{y_i}{\overline{P}_0}\right) f_{x_i}(y)\mathrm{d}y \\ &= 1 - \exp\left(-x\frac{N_0\Delta f}{\overline{P}_0}\right)\prod_{i=1}^{r}\left(1 + x\frac{\overline{P}_i}{\overline{P}_0}\right)^{-1}. \end{aligned} \tag{37}$$

APPENDIX B
PROOF OF THEOREM 2

For the moment, let as assume that the number of interfering FBSs is equal to N and that they are uniformly distributed in a circular area of radius R around the position of the user. Furthermore, in order to simplify notation, let us drop the user class and subcarrier indices. As a result of the ordering process, the order statistics $\{d_u^{(j)}\}_{j=1}^{N}$ are no longer i.i.d. and their probability density function (PDF) is given by [32]

$$f_{d_u^{(j)}}(x) = \frac{N!}{(j-1)!(N-j)!}F_d(x)^{j-1}(1-F_d(x))^{N-j}f_d(x), \tag{38}$$

for all $j \in \{1,\ldots,N\}$, where

$$f_d(x) = \begin{cases} \dfrac{2x}{R^2} = \dfrac{2\pi\lambda x}{N}, & 0 \le x \le R \\ 0, & \text{otherwise}, \end{cases} \tag{39}$$

and

$$F_d(x) = \begin{cases} 0, & x < 0 \\ \dfrac{x^2}{R^2} = \dfrac{\pi\lambda x^2}{N}, & 0 \le x \le R \\ 1, & x > R, \end{cases} \tag{40}$$

denote, respectively, the PDF and cumulative distribution function (CDF) common to all the unordered statistics $\{d_{j,u}\}_{j=1}^{N}$. Now, taking $N \to \infty$ (and thus $R \to \infty$) while keeping λ constant yields

$$f_{d_u^{(j)}}(x) = \frac{2\pi\lambda x}{(j-1)!}(\pi\lambda x^2)^{j-1}e^{-\pi\lambda x^2}, \quad x > 0. \tag{41}$$

For a user located inside a building with femtocell coverage, the conditional PDF of $d_u^{(1)}|d_u^{(1)} \le R_f$ can be obtained as

$$\begin{aligned} f_{d_u^{(1)}[q]|d_u^{(1)}\le R_f}(x) &= \frac{Pr\{d_u^{(1)} = x, d_u^{(1)} \le R_f\}}{Pr\{d_u^{(1)} \le R_f\}} \\ &= \begin{cases} \dfrac{2\pi\lambda x e^{-\pi\lambda x^2}}{1 - e^{-\pi\lambda R_f^2}}, & 0 \le x \le R_f \\ 0, & \text{otherwise}, \end{cases} \end{aligned} \tag{42}$$

and therefore, the expected distance of the nearest FBS for this particular case is

$$\mathbb{E}\left\{d_u^{(1)}|d_u^{(1)} \le R_f\right\} = \frac{R_f}{1 - e^{\pi\lambda R_f^2}} - \frac{e^{\pi\lambda R_f^2}\,\mathrm{erf}\left(\sqrt{\pi\lambda}R_f\right)}{2\sqrt{\pi}(1 - e^{\pi\lambda R_f^2})}, \tag{43}$$

where $\mathrm{erf}(\cdot)$ denotes the Gauss error function. Analogously, for a user located outside areas with femtocell coverage, the conditional PDF of $d_u^{(1)}|d_u^{(1)} > R_f$ can be obtained as

$$\begin{aligned} f_{d_u^{(1)}|d_u^{(1)}>R_f}(x) &= \frac{Pr\{d_u^{(1)} = x, d_u^{(1)} > R_f\}}{Pr\{d_u^{(1)} > R_f\}} \\ &= \begin{cases} 0, & x \le R_f \\ \dfrac{2\pi\lambda x e^{-\pi\lambda x^2}}{e^{-\pi\lambda R_f^2}}, & x > R_f. \end{cases} \end{aligned} \tag{44}$$

In this case, the expected distance of the nearest FBS can be expressed as

$$\mathbb{E}\left\{d_u^{(1)}|d_u^{(1)} > R_f\right\} = R_f + \frac{e^{\pi\lambda R_f^2}\,\mathrm{erfc}\left(\sqrt{\pi\lambda}R_f\right)}{2\sqrt{\pi}}, \tag{45}$$

where $\mathrm{erfc}(\cdot)$ is the complementary Gauss error function.

The joint PDF of the order statistics $d_u^{(1)}$ and $d_u^{(j)}$, $1 < j \le N$, is given by [32]

$$\begin{aligned} &f_{d_u^{(1)},d_u^{(j)}}(y,x) \\ &\quad= \frac{N!\,[F_d(x) - F_d(y)]^{j-2}\,[1 - F_d(x)]^{N-j}f_d(y)f_d(x)}{(j-2)!(N-j)!}, \end{aligned} \tag{46}$$

for $0 \le y < x \le R$. Again, taking $N \to \infty$ (and thus $R \to \infty$) while keeping λ constant yields

$$f_{d_u^{(1)},d_u^{(j)}}(y,x) = \frac{4(\pi\lambda)^2 yx}{(j-2)!}\left[\pi\lambda\left(x^2 - y^2\right)\right]^{j-2}e^{-\pi\lambda x^2}, \tag{47}$$

with $0 \leq y < x \leq \infty$. For a user u located inside a building with femtocell coverage then

$$f_{d_u^{(j)}|d_u^{(1)}\leq R_f}(x) = \frac{Pr\{d_u^{(j)} = x, d_u^{(1)} \leq R_f\}}{Pr\{d_u^{(1)} \leq R_f\}} = \begin{cases} 0, & x < 0 \\ \frac{2(\pi\lambda)^j x^{2j-1} e^{-\pi\lambda x^2}}{(j-1)!\left(1-e^{-\pi\lambda R_f^2}\right)}, & 0 \leq x \leq R_f \\ \frac{2(\pi\lambda)^j \left[x^{2j-1} - x\left(x^2-R_f^2\right)^{j-1}\right] e^{-\pi\lambda x^2}}{(j-1)!\left(1-e^{-\pi\lambda R_f^2}\right)}, & x > R_f. \end{cases} \quad (48)$$

Consequently, the expected distance of the jth nearest interfering FBS, with $j \geq 2$, from an user located in a building with femtocell coverage can be derived as

$$\begin{aligned} &\mathbb{E}\left\{d_u^{(j)} | d_u^{(1)} \leq R_f\right\} \\ &= \int_0^\infty x f_{d_u^{(j)}|d_u^{(1)}\leq R_f}(x) \\ &= \frac{\Gamma(j+1/2)}{\sqrt{\pi\lambda}\,(j-1)!\,\left(1-e^{-\pi\lambda R_f^2}\right)} \\ &\quad - \frac{(\pi\lambda)^j R_f^{2j+1} e^{-\pi\lambda R_f^2} U\left(j, j+3/2, \pi\lambda R_f^2\right)}{1-e^{-\pi\lambda R_f^2}}, \end{aligned} \quad (49)$$

where $\Gamma(\cdot)$ is the Gamma function and $U(\cdot,\cdot,\cdot)$ is the confluent hypergeometric function of the second kind, also known as the Kummer's function of the second kind.

Analogously, for a MU u located outside areas with femtocell coverage we have that

$$f_{d_u^{(j)}|d_u^{(1)}>R_f}(x) = \frac{Pr\{d_u^{(j)} = x, d_u^{(1)} > R_f\}}{Pr\{d_u^{(1)} > R_f\}} = \begin{cases} 0, & x \leq R_f \\ \frac{2(\pi\lambda)^j x \left(x^2-R_f^2\right)^{j-1}}{(j-1)!\, e^{\pi\lambda\left(x^2-R_f^2\right)}}, & x > R_f, \end{cases} \quad (50)$$

and thus, the expected distance of the jth nearest interfering FBS, with $j \geq 2$, is given by

$$\begin{aligned} \mathbb{E}\left\{d_u^{(j)} | d_u^{(1)} > R_f\right\} &= \int_{R_f}^\infty x f_{d_u^{(j)}|d_u^{(1)}>R_f}(x)\,\mathrm{d}x \\ &= (\pi\lambda)^j R_f^{2j+1} U\left(j, j+3/2, \pi\lambda R_f^2\right). \end{aligned} \quad (51)$$

REFERENCES

[1] E. Dahlman, S. Parkvall, and J. Skold, *4G: LTE/LTE-Advanced for Mobile Broadband*, 2nd ed. Amsterdam, The Netherlands: Elsevier, 2013.

[2] J. G. Andrews *et al.*, "What will 5G be?" *IEEE J. Sel. Areas Commun.*, vol. 32, no. 6, pp. 1065–1082, Jun. 2014.

[3] A. S. Hamza, S. S. Khalifa, H. S. Hamza, and K. Elsayed, "A survey on inter-cell interference coordination techniques in OFDMA-based cellular networks," *IEEE Commun. Surveys Tuts.*, vol. 15, no. 4, pp. 1642–1670, 4th Quart., 2013.

[4] H. Lei, L. Zhang, X. Zhang, and D. Yang, "A novel multi-cell OFDMA system structure using fractional frequency reuse," in *Proc. IEEE Int. Symp. Pers., Indoor Mobile Radio Commun. (PIMRC)*, Sep. 2007, pp. 1–5.

[5] N. Saquib, E. Hossain, and D. I. Kim, "Fractional frequency reuse for interference management in LTE-advanced hetnets," *IEEE Wireless Commun.*, vol. 20, no. 2, pp. 113–122, Apr. 2013.

[6] J. G. Andrews, "Seven ways that HetNets are a cellular paradigm shift," *IEEE Commun. Mag.*, vol. 51, no. 3, pp. 136–144, Mar. 2013.

[7] T. Zahir, K. Arshad, A. Nakata, and K. Moessner, "Interference management in femtocells," *IEEE Commun. Surveys Tuts.*, vol. 15, no. 1, pp. 293–311, 1st Quart., 2013.

[8] D. Calin, H. Claussen, and H. Uzunalioglu, "On femto deployment architectures and macrocell offloading benefits in joint macro-femto deployments," *IEEE Commun. Mag.*, vol. 48, no. 1, pp. 26–32, Jan. 2010.

[9] A. Ghosh *et al.*, "Heterogeneous cellular networks: From theory to practice," *IEEE Commun. Mag.*, vol. 50, no. 6, pp. 54–64, Jun. 2012.

[10] M. Taranetz, J. C. Ikuno, and M. Rupp, "Sensitivity of OFDMA-based macrocellular LTE networks to femtocell deployment density and isolation," in *Proc. 10th Int. Symp. Wireless Commun. Sys. (ISWCS)*, Aug. 2013, pp. 1–5.

[11] J. G. Andrews, F. Baccelli, and R. K. Ganti, "A tractable approach to coverage and rate in cellular networks," *IEEE Trans. Commun.*, vol. 59, no. 11, pp. 3122–3134, Nov. 2011.

[12] A. Guo and M. Haenggi, "Spatial stochastic models and metrics for the structure of base stations in cellular networks," *IEEE Trans. Wireless Commun.*, vol. 12, no. 11, pp. 5800–5812, Nov. 2013.

[13] H. Elsawy, E. Hossain, and M. Haenggi, "Stochastic geometry for modeling, analysis, and design of multi-tier and cognitive cellular wireless networks: A survey," *IEEE Commun. Surveys Tuts.*, vol. 15, no. 3, pp. 996–1019, 3rd Quart., 2013.

[14] R. W. Heath, Jr., M. Kountouris, and T. Bai, "Modeling heterogeneous network interference using Poisson point processes," *IEEE Trans. Signal Process.*, vol. 61, no. 16, pp. 4114–4126, Aug. 2013.

[15] T. D. Novlan, R. K. Ganti, A. Ghosh, and J. G. Andrews, "Analytical evaluation of fractional frequency reuse for OFDMA cellular networks," *IEEE Trans. Wireless Commun.*, vol. 10, no. 12, pp. 4294–4305, Dec. 2011.

[16] T. D. Novlan, R. K. Ganti, A. Ghosh, and J. G. Andrews, "Analytical evaluation of fractional frequency reuse for heterogeneous cellular networks," *IEEE Trans. Commun.*, vol. 60, no. 7, pp. 2029–2039, Jul. 2012.

[17] F. Jin, R. Zhang, and L. Hanzo, "Fractional frequency reuse aided twin-layer femtocell networks: Analysis, design and optimization," *IEEE Trans. Commun.*, vol. 61, no. 5, pp. 2074–2085, May 2013.

[18] M. Assaad, "Optimal fractional frequency reuse (FFR) in multicellular OFDMA system," in *Proc. IEEE 68th Veh. Technol. Conf. (VTC-Fall)*, Sep. 2008, pp. 1–5.

[19] A. Najjar, N. Hamdi, and A. Bouallegue, "Efficient frequency reuse scheme for multi-cell OFDMA systems," in *Proc. IEEE Symp. Comput. Commun. (ISCC)*, Jul. 2009, pp. 261–265.

[20] Z. Xu, G. Y. Li, C. Yang, and X. Zhu, "Throughput and optimal threshold for FFR schemes in OFDMA cellular networks," *IEEE Trans. Wireless Commun.*, vol. 11, no. 8, pp. 2776–2785, Aug. 2012.

[21] G. Femenias and F. Riera-Palou, "Corrections to and comments on 'throughput and optimal threshold for FFR schemes in OFDMA cellular networks,'" *IEEE Trans. Wireless Commun.*, vol. 14, no. 5, pp. 2926–2928, May 2015.

[22] J. García-Morales, G. Femenias, and F. Riera-Palou, "Performance analysis and optimisation of FFR-aided OFDMA networks using channel-aware scheduling," *Mobile Netw. Appl.*, pp. 1–15, May 2016, doi: 10.1007/s11036-016-0730-8.

[23] V. Chandrasekhar and J. G. Andrews, "Spectrum allocation in tiered cellular networks," *IEEE Trans. Commun.*, vol. 57, no. 10, pp. 3059–3068, Oct. 2009.

[24] J. Xiang, Y. Zhang, T. Skeie, and L. Xie, "Downlink spectrum sharing for cognitive radio femtocell networks," *IEEE Syst. J.*, vol. 4, no. 4, pp. 524–534, Dec. 2010.

[25] X. Kang, R. Zhang, and M. Motani, "Price-based resource allocation for spectrum-sharing femtocell networks: A Stackelberg game approach," *IEEE J. Sel. Areas Commun.*, vol. 30, no. 3, pp. 538–549, Apr. 2012.

[26] H. Zhang, C. Jiang, N. C. Beaulieu, X. Chu, X. Wen, and M. Tao, "Resource allocation in spectrum-sharing OFDMA femtocells with heterogeneous services," *IEEE Trans. Commun.*, vol. 62, no. 7, pp. 2366–2377, Jul. 2014.

[27] H. Zhang, C. Jiang, X. Mao, and H.-H. Chen, "Interference-limited resource optimization in cognitive femtocells with fairness and imperfect spectrum sensing," *IEEE Trans. Veh. Technol.*, vol. 65, no. 3, pp. 1761–1771, Mar. 2016.

[28] J. García-Morales, G. Femenias, and F. Riera-Palou, "Analytical performance evaluation of OFDMA-based heterogeneous cellular networks using FFR," in *Proc. IEEE Veh. Technol. Conf. (VTC Spring)*, May 2015, pp. 1–7.
[29] *Home eNode B (HeNB) Radio Frequency (RF) Requirements Analysis (Release 9), v9.0.0.*, document TR36.921, Mar. 2010.
[30] A. Mawira, "Estimate of mean C/I and capacity of interference limited mobile ad-hoc networks," in *Proc. IEEE Int. Zurich Seminar Broadband Commun.*, Feb. 2002, pp. 51-1–51-6.
[31] M. Maqbool, P. Godlewski, M. Coupechoux, and J.-M. Kélif, "Analytical performance evaluation of various frequency reuse and scheduling schemes in cellular OFDMA networks," *Perform. Eval.*, vol. 67, no. 4, pp. 318–337, Apr. 2010.
[32] H. A. David, *Order Statistics*. New York, NY, USA: Wiley, 1981.

JAN GARCÍA-MORALES (S'14) was born in Cienfuegos, Cuba, in 1984. He received the degree in telecommunications and electronic from the Faculty of Electrical Engineering, Central University of Las Villas, Villa Clara, Cuba, in 2008, and the M.S. degree in information technologies from the Department of Mathematical and Information, University of the Balearic Islands, in 2013. He is currently pursuing the Ph.D. degree in information and communication technologies with the Higher Polytechnic School, University of the Balearic Islands. He is working on his thesis project: "Heterogeneous multi-tier networks, towards ubiquitous multimedia content distribution", and under the group research line: "Resource management in mobile communications networks". He was with Mobile Telecommunications Company MOVITEL S.A. from 2008 to 2012. Motivated by the research in the telecommunications and information technology area, he applied for one of the Santander-Iberoamerica scholarship in 2012 to study the master's degree (research itinerary) in Spain. Upon completion of the M.Sc., he stayed with Innovation and Technology Company IBITEC S.L. as a Santander-Crue-Cepyme Internship Researcher Assistant conducting work on designing and programming automatic systems and sensor networks. In 2013, he obtained a pre-doctorate scholarship under project AM3DIO (TEC2011-25446). He is a member of the Mobile Communications Group.

GUILLEM FEMENIAS (SM'11) received the Telecommunication Engineer degree and the Ph.D. degree in electrical engineering from the Technical University of Catalonia (UPC), Barcelona, Spain, in 1987 and 1991, respectively. From 1987 to 1994, he was a Researcher with UPC, where he became an Associate Professor in 1992. In 1995, he joined the Department of Mathematics and Informatics, University of the Balearic Islands (UIB), Mallorca, Spain, where he became a Full Professor in 2010. He is currently leading the Mobile Communications Group at UIB, where he has been the Project Manager of projects ARAMIS, DREAMS, DARWIN, MARIMBA, COSMOS, and ELISA, all of them funded by the Spanish and Balearic Islands Governments. In the past, he was also involved in several European projects (ATDMA, CODIT, and COST). His current research interests and activities span the fields of digital communications theory and wireless communication systems, with particular emphasis on cross-layer transceiver design, resource management, and scheduling strategies applied to fourth- and fifth-generation wireless networks. On these topics, he has published more than 90 journal and conference papers, as well as some book chapters. He was a recipient of the Best Paper Awards at the 2007 IFIP International Conference on Personal Wireless Communications and at the 2009 IEEE Vehicular Technology Conference-Spring. He has served for various IEEE conferences as a Technical Program Committee Member, as the Publications Chair for the IEEE 69th Vehicular Technology Conference (Spring 2009), and as the Local Organizing Committee Member of the IEEE Statistical Signal Processing (2016).

FELIP RIERA-PALOU (SM'11) was born in Mallorca, Spain, in 1973. He received the B.S./M.S. degree in computer engineering from the University of the Balearic Islands (UIB), Mallorca, in 1997, the M.Sc. and Ph.D. degrees in communication engineering from the University of Bradford, U.K., in 1998 and 2002, respectively, and the M.Sc. degree in statistics from the University of Sheffield, U.K., in 2006. From 2002 to 2005, he was with Philips Research Laboratories, Eindhoven, The Netherlands, first as a Marie Curie Post-Doctoral Fellow (European Union) and later as a member of the Technical Staff. While at Philips, he worked on research programs related to wideband speech/audio compression and speech enhancement for mobile telephony. From 2005 to 2009, he was a Research Associate (Ramon y Cajal program, Spanish Ministry of Science) with the Mobile Communications Group, Department of Mathematics and Informatics, UIB. Since 2010, he has been an Associate Research Professor (I3 program, Spanish Ministry of Education) at UIB. His current research interests are in the general areas of signal processing and wireless communications.